Bioactive tri-component nanofibers from cellulose acetate/lignin//N-vanillidene-phenylthiazole copper-(II) complex for potential diaper dermatitis control

International Journal of Biological Macromolecules 205 (2022) 703–718

Contents lists available at ScienceDirect

International Journal of Biological Macromolecules

journal homepage: www.elsevier.com/locate/ijbiomac

Bioactive tri-component nanofibers from cellulose acetate/lignin// N-vanillidene-phenylthiazole copper-(II) complex for potential diaper dermatitis control

Dalia A. Elsherbiny [a,b], Abdelrahman M. Abdelgawad [c,*], Mehrez E. El-Naggar [c,d,*], Bahaa A. Hemdan [e], Samaneh Ghazanfari [b,f], Stefan Jockenhövel [b,f], Orlando J. Rojas [d,g]

[a] Menoufia University, Faculty of Science, Chemistry Department, Shebin El-Koom, Menoufia, Egypt
[b] Aachen-Maastricht Institute for Biobased Materials, Faculty of Science and Engineering, Maastricht University, the Netherlands
[c] Textile Research and Technology Institute, National Research Centre, 33 El-Bohouth St., Dokki, Giza 12622, Egypt
[d] Department of Forest Biomaterials, College of Natural Resources, North Carolina State University, Raleigh, NC 27607, USA
[e] Water Pollution Research Department, National Research Centre, 33 El-Bohouth St., Dokki, Giza 12622, Egypt
[f] Department of Biohybrid & Medical Textiles (BioTex), AME-Helmholtz Institute for Biomedical Engineering, RWTH Aachen University, Forckenbeckstrabe 55, 52072 Aachen, Germany
[g] Bioproducts Institute, Department of Chemical & Biological Engineering, 2360 East Mall, The University of British Columbia, Vancouver, BC V6T 1Z3, Canada

ARTICLE INFO

Keywords:
Cellulose acetate
Lignin
Electrospinning
Antibacterial
Diaper dermatitis

ABSTRACT

Current research targets innovative medical textiles of nanofibrous nature and antibacterial activity to prevent diaper dermatitis. The work is based on electrospun nanofibers from cellulose acetate (CA) and lignin (Lig) polymers. A series of new copper complexes were synthesized and loaded to the CA/Lig solution mix then subjected to electrospinning, giving rise to the tricomponent bioactive mats CA/Lig/Cu-complex. The surface morphology of electrospun nanofiber mats was smooth and homogenous as the concentration of lignin increased in the mixture. The incorporation of lignin improved the electrospinnability of the cellulose acetate; however, it increased the fiber diameter. The water contact angle, absorption underload were significantly improved as lignin content increased. The incorporation of Cu-complex in electrospun CA and CA/Lig fiber mats occurred without any substantial change in the surface morphology, indicating well encapsulation of the complex. The electrospun mats were active against *Pseudomonas aeruginosa*, *Acinetobacter baumannii*, *Staphylococcus epidermidis*, and *Streptococcus faecalis*. The cytotoxicity, protein leakage, and biological results, together with the above studies, would advocate copper complex loaded CA/Lig nanofibers as a potential candidate for hygienic applications.

1. Introduction

Diaper dermatitis (DD) is a skin inflammation that develops unexpectedly under the diaper region [1,2]. This is a persisting problem in young children but more severe in elderly patients who suffer from urine incontinent illness. For the most part, patients with urine incontinent problems fail to control the discharge of urine and excrement [3,4]; therefore, collecting articles such as fiber pads or diapers is recommended. The primary function of such materials is to absorb and retain discharged fluids, isolate them from the skin, prevent odor, and maintain comfort. Consequently, the collecting articles usually constitute several layers such as cover, acquisition and distribution, absorbent core, back sheet, tissue, and siliconized paper layers. Usually, the absorbent core layer is responsible for the fluid holding capacity made from cellulosic wood pulp fibers [5].

In general, the risk of microbial infections is high as in old age and weak immunity patients. Moreover, the potential of microbial growth increases due to the development of skin ulcers from continuous mechanical friction between the skin and the absorbing material [2]. As a result, the urine concentrates in the absorbing articles and gets warm for a long time because of its close contact with the body, which creates a conducive atmosphere for fungal and bacterial growth [6]. Such conditions stimulate DD in most cases. The most common skin microbial species frequently associated with DD are *Candida albicans* and bacteria

* Corresponding authors.
E-mail addresses: aabdelgawad@gmail.com, aabdelg@ncsu.edu (A.M. Abdelgawad), mehrez_chem@yahoo.com (M.E. El-Naggar).

https://doi.org/10.1016/j.ijbiomac.2022.02.192
Received 22 January 2022; Received in revised form 6 February 2022; Accepted 28 February 2022
Available online 4 March 2022

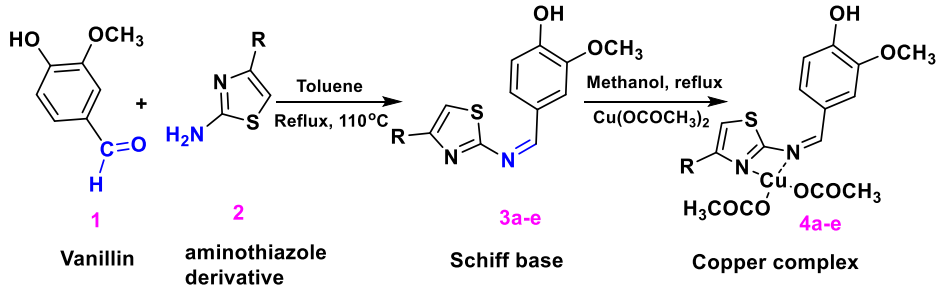

Comp. no.	R	Amine Name	Code
a	H	thiazol-2-amine	**Cu-Amine**
b	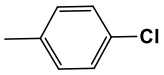	4-(4-chlorophenyl)thiazol-2-amine	**Cu-Cl**
c	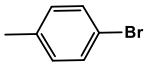	4-(4-bromophenyl)thiazol-2-amine	**Cu-Br**
d	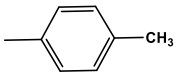	4-(p-tolyl)thiazol-2-amine	**Cu-Tolyl**
e	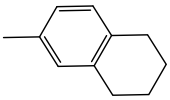	4-(5,6,7,8-tetrahydronaphthalen-2-yl)thiazol-2-amine	**Cu-Tetrahydro**

Scheme 1. Synthesis of Cu(II) complexes; the reaction of vanillin with different thiazole amine derivatives and the chemical structures of the starting amines.

like *Staphylococcus aureus* (-hemolytic), *Staphylococcus epidermidis*, *Streptococcus* sp., *Acinetobacter baumannii*, *Pseudomonas aeruginosa*, *E. coli*, and *Bacteroides* sp. [7,8].

Therefore, there is a need to acquire antimicrobial properties to the absorption core of collecting diapers to lessen the risk of microbial infections. Different strategies for developing effective germicidal fibers and textile protective layers for hygienic applications have been published in the literature [9]. For example, Jia-Horng et al. utilized quaternary ammonium salts to develop caretaking for urinary incontinence of cotton fibers [10]. In addition, silver nanoparticles, zinc oxide nanoparticles, and natural products like curcumin were tested as practical germicidal components in diapers [11–14]. The antibacterial activities of vanillin Schiff bases, particularly those containing thiazole ring systems, were studied before in the literature [15,16]. Condensation of aminothiazole with Vanillin produces a bioactive bidentate ligand, which helps form a series of complexes with some transition metal ions like copper. Such copper complexes are well known for their antimicrobial activities [17].

Nanofibers exhibit exceptional properties compared to other morphologies due to high pore volume and high surface area-to-weight ratio [18–20]. Several polymers can be processed to produce nanofibers using methods such as electrospinning, solution blowing, phase separation, and template-assisted fabrication [21,22]. However, electrospinning is a simple and straightforward method to fabricate fibers with diameters in the submicron and nanometer range [23,24]. In the conventional electrospinning process, a high electrostatic voltage is forced on polymer solution drop, held by a reverse force, its surface tension, at the end of an injection needle. As a result, the surface of the liquid is deployed into a conical shape known as the Taylor cone. When the imposed voltage surpasses a critical value, the electrostatic force overcomes the droplet surface tension and a stable liquid polymer jet is spins from the cone tip. Ultrafine fibers with small pore sizes are collected on a grounded target as the solvent evaporates and the jet travels from the tip of the needle, through air, towards a grounded target [25–27]. Therefore, it finds many applications in drug delivery, medical protective textiles, and superabsorbent material in feminine hygiene products [28–30].

Cellulose acetate (CA) is a biobased and biocompatible polymer prepared by chemical esterification of highly pure cellulose [31]. CA nanofibers have been investigated in different biomedical applications due to their biocompatibility, easy processability, and low price [32]. Unlike cellulose, CA is spinnable from volatile organic solvents, making it more suitable for electrospinning. In addition, it shows hydrolytic stability and offers more excellent water retention under pressure than native cellulose wood-pulp fibers [33]. Sharma et al., proved the potential use of cellulose acetate nanofibers in feminine hygiene pads and sanitary napkins [30]. They found that water and urine equilibrium absorbency and absorbency under-load of CA nanofibers outperformed the conventional cellulosic wood-pulp core due to their large surface-

Table 1
Electrospinning solutions from polymer blends of cellulose acetate and lignin in Acetone/DMAc solvent system.

Sample code	Cellulose acetate (CA) content in 100 mL solvent (g)	The solid content of lignin (Lig) in 100 mL solvent (g)	Lignin percentage (relative to CA weight) %	CA:Lig The ratio in 100 mL solvent
L0	7	0	0	100:0
L17	7	1.4	20	83:17
L29	7	2.8	40	71:29
L 37	7	4.2	60	62.3:37.5
L44	7	5.6	80	55.6:44.4
L50	7	7	100	50:50

area and high porosity. However, we still see room for improvement in the absorption capacity of CA nanofibers.

CA properties depend on its esterification degree, the number of substituted hydroxyl groups, which specify the obtained material like acetate, diacetate, or triacetate [34]. Therefore, CA holds some hydrophobic properties due to replacing cellulose hydrophilic hydroxyl groups. Hence, we propose blending lignin with cellulose acetate to boost its water uptake capacity. Lignin acquires some water affinity after pulping due to the presence sulfonate group residuals in its structure. It is considered the second most abundant biomaterial in nature. Moreover, its use is economically feasible since it is produced as a side-product of the pulp and paper and cellulosic biofuel industries. According to the Food and Agricultural Organization of the United Nations (FAO) report, the worldwide lignin production reached 100M tonnes per year, with a value of $732.7 million in 2015, and is expected to reach $913M by 2025 [35].

In the present study, experiments are designed to fabricate a protective layer from cellulose acetate/lignin/copper-complex nanofibers using the conventional electrospinning method to control diaper dermatitis. Five novel N-vanillidene-2-amino-thiazole Schiff base derivatives were synthesized, and their copper complexes were prepared. The as-prepared complexes' antibacterial activity and biocompatibility were investigated against five skin pathogenic bacterial lineages; *Pseudomonas aeruginosa*, *Acinetobacter baumannii*, *Staphylococcus epidermidis*, and *Streptococcus faecalis*. The compound with the highest efficiency and less cytotoxicity was selected for application onto the nanofiber system. Furthermore, the electrospinning of cellulose acetate/lignin nanofibers was optimized by studying different polymer blends. To the authors' knowledge, neither the cellulose acetate/lignin system nor the prepared copper complexes were discussed previously in the literature as medicated absorbing articles. Therefore, we believe it brought a promising protecting and effective fibrous layer for various hygienic applications. FTIR, NMR, and UV–vis spectroscopy illustrated the chemical structures of the synthesized copper complexes. Also, the morphology and thermal behavior of the electrospun nanofibers were examined by scanning electron microscope (SEM), thermal gravimetric analysis (TGA), respectively. In addition, its capacity as a fluid absorbent was assessed by studying the equilibrium absorption and the absorption under load. Finally, the antibacterial activity and bioburden of the functionalized nanofibers were examined.

2. Experimental

2.1. Materials

Cellulose diacetate (a white powder; Mw 50,000, degree of substitution ("DS") from about 1.0 to about 2.8 (acetyl: 39.8% and hydroxyl: 3.5%)) was donated from Eastman Chemicals, USA. Sulfonate-lignin (Lig) was a technical grade softwood produced by Domtar Inc. Plymouth Pulp Mill, NC (USA). Sodium chloride, ammonium chloride, sodium phosphate, copper (II) acetate, Vanillin, 2-amino-4-(phenylthiazole) derivatives were purchased from Sigma Aldrich. Solvents such as *N*, *N*-dimethyl acetamide (DMAc), and acetone were purchased from Fisher Scientific and used as received.

2.2. Synthesis of copper-II complexes

The first step in forming copper complexes is the synthesis of Schiff bases. In general, a Schiff base is the product of an amine and an aldehyde. Herein, vanillin was reacted with thiazolamine, 4-(4-chlorophenyl)thiazolamine, 4-(4-bromophenyl)thiazolamine, 4-(p-tolyl) thiazolamine, 4-(5,6,7,8-tetrahydronaphthalenyl)thiazolamine. Then, the corresponding copper complexes were prepared by reacting the Schiff bases with a copper salt.

2.2.1. Preparation of Schiff base

The target amine (thiazole-2-amine derivatives) (presented in Scheme 1, 15.74 mmol) was suspended in 50 mL toluene (solution 1). Vanillin (15.74mmole) was suspended in 30 mL toluene (solution 2). Both solution 1 and solution 2 were heated in a three-necked flask (250 mL) placed in an oil bath to control the temperature. Solution-2 was added to solution-1 under stirring. Then, a glass condenser was placed on the flask for 6 h reflux. The solvent was evaporated and cooled down to obtain a concentrated deep orange to a brown-colored product. The product was filtered and washed with toluene, then ether, and dried under vacuum.

2.2.2. Complexation of Schiff base with copper salt

3.15 g of the Schiff base was dissolved in 50 mL methanol under heating at 75 °C. Exactly, 0.6 g copper acetate is dissolved in 50 mL methanol under heating 75 °C. Both solutions were mixed under stirring in a three-necked flask (250 mL) (placed in an oil bath to control the temperature fluctuation). The reaction was kept running (reflux) for 4 h. After that, the solvent was evaporated and cooled down. Then, the deep brown color is concentrated (copper II complex). Finally, the product was filtered, washed with dry methanol, ether, and further dried under a vacuum.

Five copper complexes (Cu-complex) were prepared, chemically characterized, and their antibacterial efficiency was screened against the aforementioned bacterial strains. Finally, the most efficient complex was selected to load fibers and produce the antibacterial protective layer.

2.3. Preparation of electrospinning solutions

Nonwoven nanofibers meshes from CA, CA/lignin, and CA/lignin/Cu-complex were produced by electrospinning. The desired polymer blending conditions are described in Table 1. Samples are coded according to their lignin content. A specific amount of CA was dissolved in acetone/DMAc (2:1 v/v) to obtain a 7% (w/v) concentration solution, coded as Lig 0. For electrospinning of CA/lignin, five different concentrations of lignin 20%, 40%, 60%, 80%, and 100% (relative to the weight of CA) into the CA solution under continuous stirring for 4 h prior to the spinning process. For loading the electrospinning solution with the cupper complex drug, 0.5% was added to the selected solution; which provided bead-free and uniform fiber morphology and contains the highest lignin content, under contentious stirring until complete solubility.

2.4. Electrospinning process

Each CA or CA/lignin and CA/lignin/Cu-complex was loaded into a plastic 20 mL syringe. Then, electrospinning was carried out by connecting the electrode from a high voltage direct current power supply to the syringe. The open end of the syringe was plugged with a blunt stainless steel needle (gauge-20, diameter 0.9 mm). The grounding electrode was attached to the fiber collector (diameter around 20 cm).

Table 2
FTIR spectral data of Cu(II) acetate-based complexes.

Compounds: [Cu (II) acetate-based complexes]	Assignments					
	Azo-methine ν(C=N)	Ring ν(C=N)	ν (C=C, Ar.)	ν (-OH)	ν(C-S-C)	Yield
Cu-amine	1663	1600	1419	3363	628	85%
Cu-Cl	1603	1558	1427	3317	632	82%
Cu-Br	1667	1592	1425	3361	633	87%
Cu-tolyl	1668	1581	1426	3358	632	85%
Cu-tetrahydro	1670	1596	1426	3361	630	89%

An automated syringe pump was employed to feed the solution at a speed of 2 mL/h. A specific electrical potential (20 kV) was applied over a defined distance of 20 cm. The samples were collected on an aluminum foil (20 cm × 20 cm) sheet. For the morphological study, the collection time was around 5 min and 24 h for the rest of the samples. Upon completing the spinning process, the fiber mats were removed from the collector and kept under dry conditions until further characterization.

2.5. Preparation of synthetic urine

Synthetic urine was used to test the fluid absorbance affinity of the electrospun fibers at equilibrium and under pressure. The testing solution was prepared according to a recipe established by Kim et al. [36]. To 1 L of distilled water, urea (25 g), sodium phosphate (2.5 g), sodium chloride (9 g), sodium sulfite (3 g), and ammonium chloride (3 g) were added and stirred for 1 h to ensure complete dissolution. The solution was kept in the fridge at 4 °C for further testing.

2.6. Chemical characterization of copper complexes

Chemical characterization of the Schiff base ligand and its copper acetate complex was performed using different analytical techniques. Attenuated Total Reflectance-Fourier Transform Infra-Red (ATR/FT-IR) spectra of the Schiff base ligand and the final Cu-II complex were obtained on a Nexus 470 FTIR Spectrophotometer (Thermo Nicolet). ^{1}H NMR spectra of the Schiff base ligand were recorded in DMSO at room temperature using Bruker 500 MHz spectrometer. Finally, mass spectrometry of the Schiff base ligand was measured using Shimadzu LCMS-2020 using methanol and acetonitrile as a mobile phase. All three devices are located at the analytical laboratory of Aachen-Maastricht Institute for Biobased Materials, Maastricht University.

2.7. Fiber morphological characterization

The fiber morphology was investigated by field emission scanning electron microscopy (FE-SEM, JEOL-6400F) equipped with an X-ray detector. The SEM operated at 5 kV and 25 mm working distance. The nanofiber sample was mounted on carbon tape support, followed by sputtering around a 5 nm layer of gold.

2.8. Fiber thermal properties

The thermal behavior of the resulting electrospun nanofibers was measured using thermal gravimetric analysis (TGA) technique under nitrogen atmosphere. A Q5000-TGA-DTA (TA-instruments, USA) in the temperature range of 40–650 °C, with a heating rate of 10 °C/min.

2.9. Change in hydrophilicity of CA/Lig nanofibers: water contact angle

The water contact angle technique was used to measure the change in hydrophilicity/hydrophobicity of the electrospun nanofibers. A micro-syringe was used at a rate of 7–10; water drops were noticed under a microscope attached to a Phoneix-SEO camera. The images were analyzed using image processors Image-XPFW012108 and Image-J-1.410.

2.10. Equilibrium absorbency and absorbency under-load (AUL)

The absorbency test was performed to estimate the absorption potency of the electrospun nanofibers when allowed to swell for 24 h freely. Electrospun nanofiber mats (0.15 mm thickness) were cut into squares of 2 × 2 cm. The sensitive scale measured the dry weight (W1). The samples were placed in a Petri dish filled with urine solution and covered for 24 h. The excess water was removed by paper tissue, and the swollen samples were weighed (W2). Equilibrium absorbency was calculated from the following formula:

$$Q = [(W2 - W1)\ W1] \times 100$$

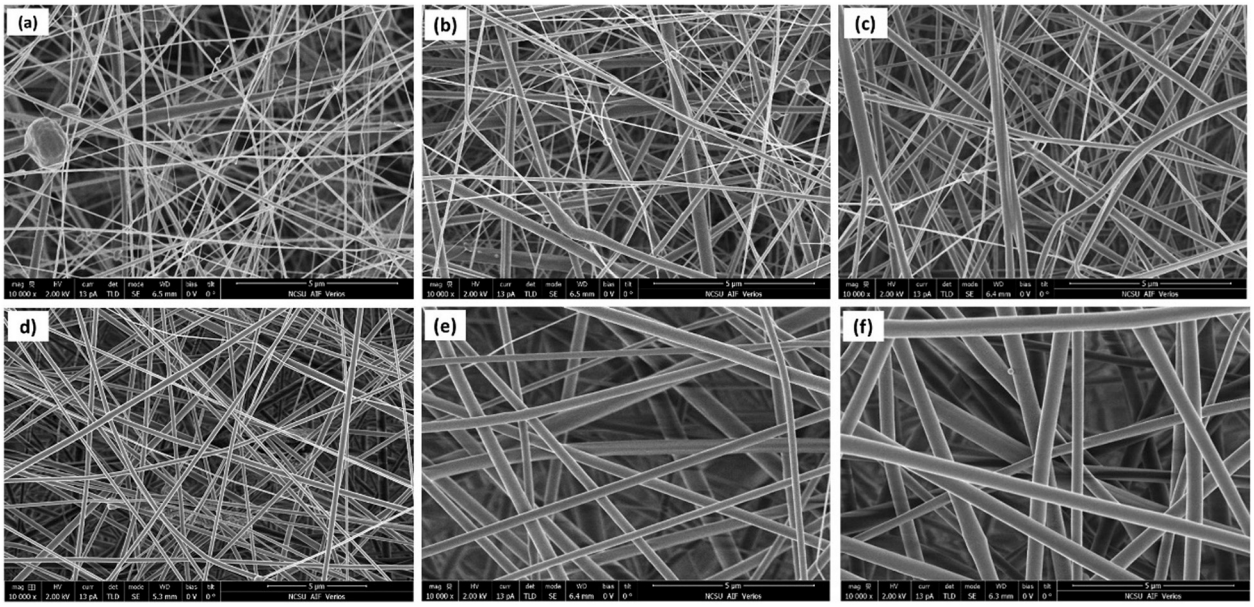

Fig. 1. SEM micrograph of as-produced CA/lignin nanocomposite fibers prepared from 7% CA and various concentrations of lignin (a) L0, (b) L17, (c) L29, (d) L37, (e) L44, and (f) L50.

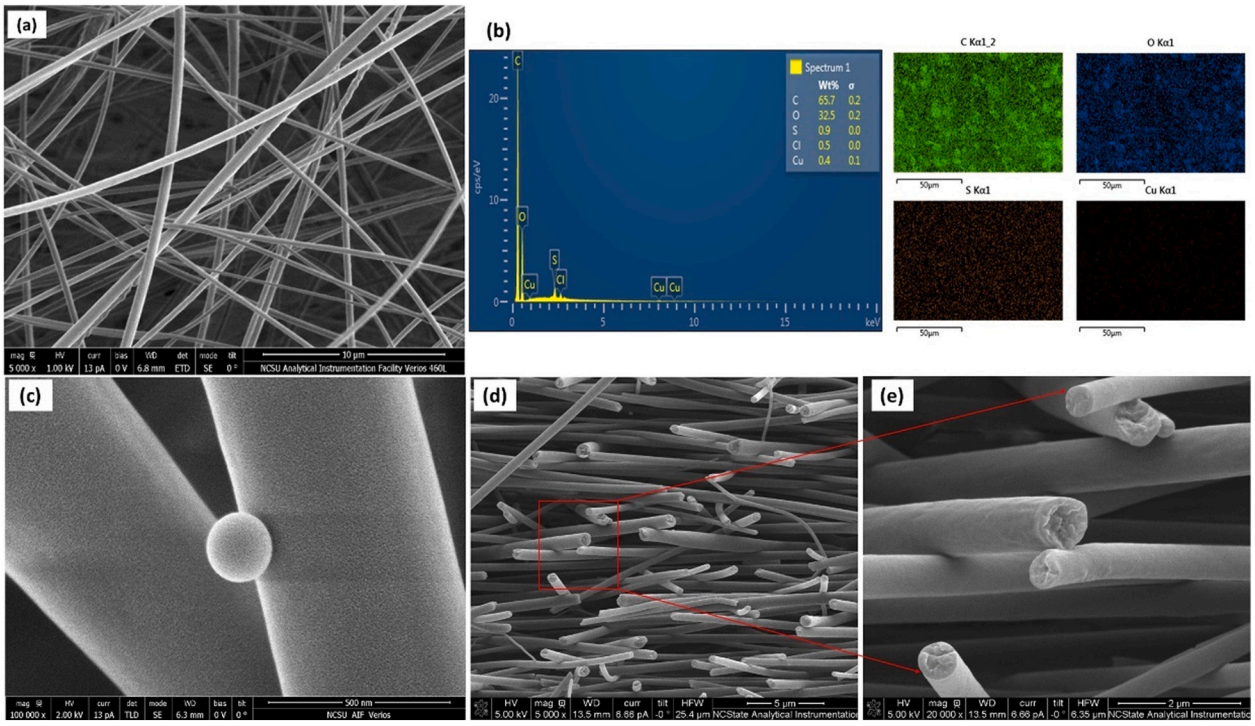

Fig. 2. (a) SEM micrograph of Cu (II) complex loaded CA/lignin nanofibers at 50:50 ratios of lignin (L50); (b) EDX chart and element mapping of L50 loaded with complex, (c) SEM micrograph of fiber surface at high magnification, (d) cross-section of L50 nanofibers, (e) zoom-in and high magnification of image (d).

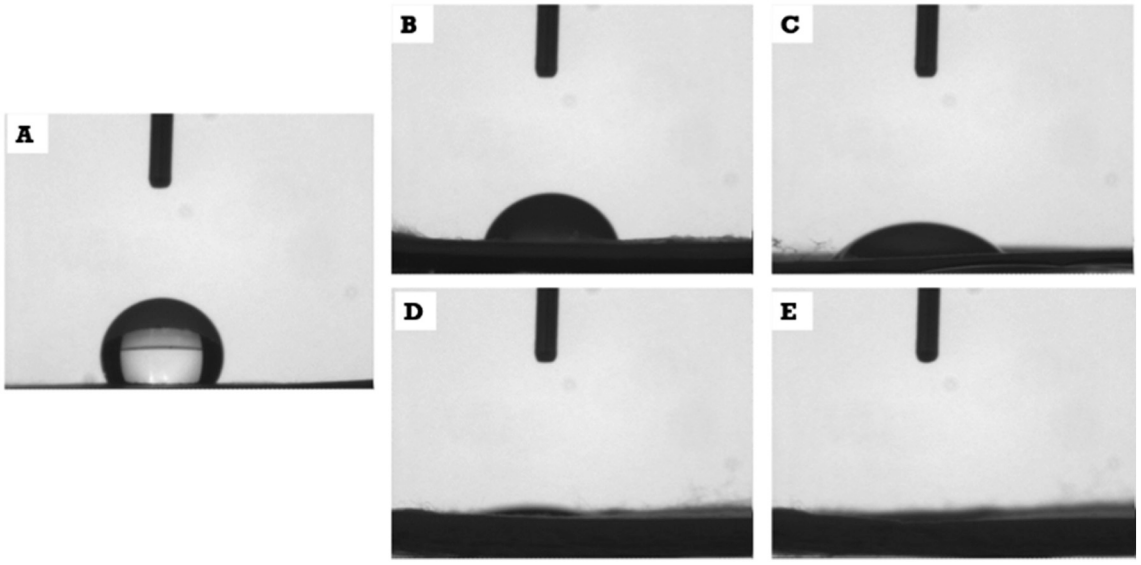

Fig. 3. Micrograph of surface contact angle of CA/Lig nanofiber mats at different lignin content (A) L0, (B) L17, (C) L29, (D) L37, (E) L44.

where Q is the percent free absorbency.

Since the collecting articles are used under load (bodyweight), the absorption capacity under load should be evaluated for the electrospun nanofibers. Generally, the AUL measures the ability of the superabsorbents to absorb a specific amount of 0.9% saline solution while being under particular pressure. The absorbency test was conducted at room temperature (27 °C) and 60% relative humidity. The setup for the AUL tester was adapted from the literature [30] with slight modification. Briefly, a petri dish is filled with synthetic urine solution, and a glass filter plate (30 mm, diameter) is placed inside. A filter paper of the same diameter was placed on the top of the plate. Then a circular shape nanofiber sample (30 mm diameter and 0.15 mm thickness) was placed on the filter paper. A specific weight (50 g) was placed in a beaker and placed on the top of the sample. The test runs for 60 min then the sample is removed and weighed. The absorbency under-load percentage was calculated from the following formula:

$$A = [(W2 - W1)\, W1\,] \times 100$$

where A is the absorbency under-load percentage; (W1) is the initial dry weight of the nanofiber mat; (W2) is the final wet weight after impregnation in urine.

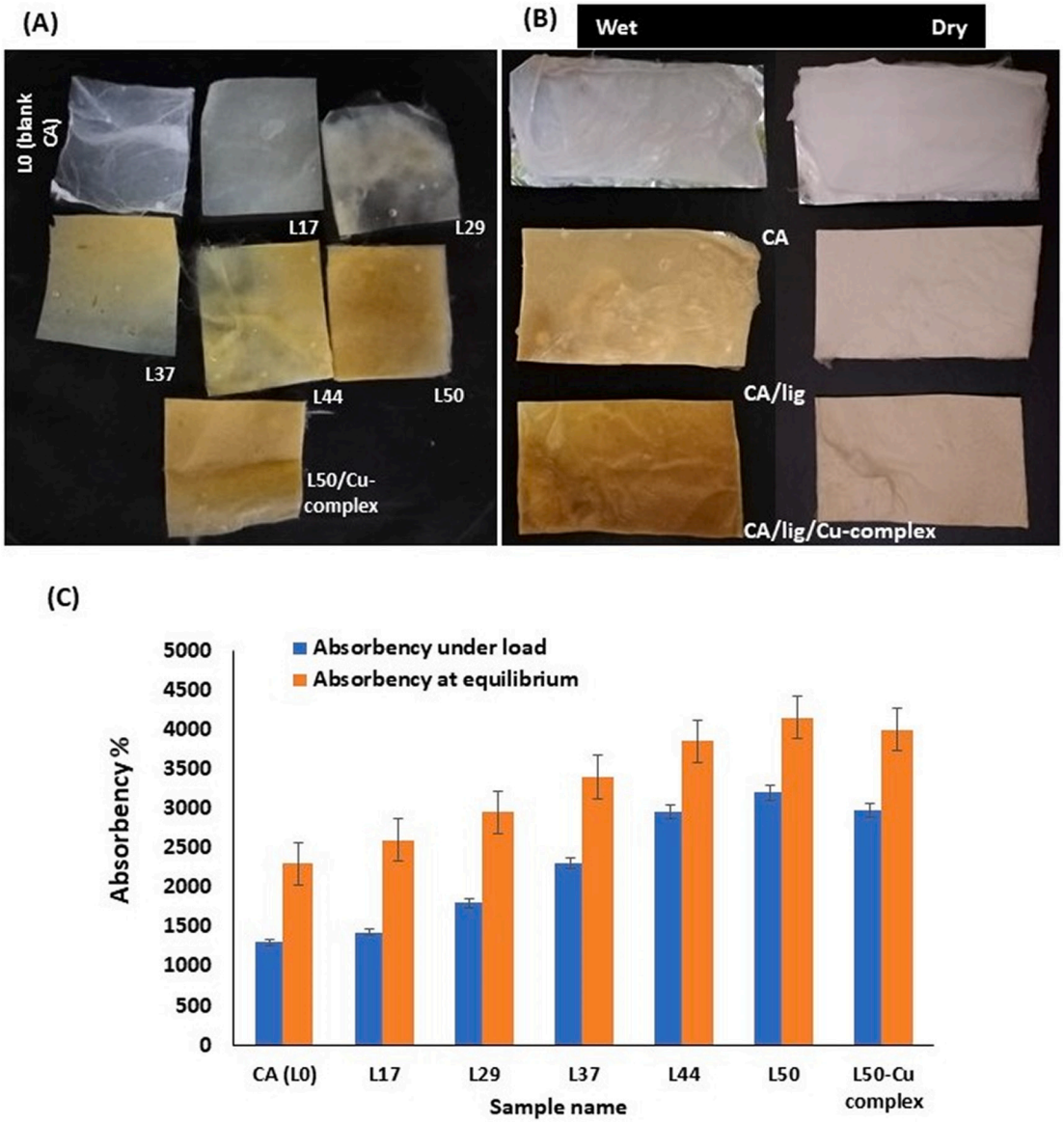

Fig. 4. (A) Absorption in synthetic urine solution, (B) Pictorial representation of nanofiber mats at equilibrium absorption in urine solution for 24 h; (C) urine absorbency and absorption under load.

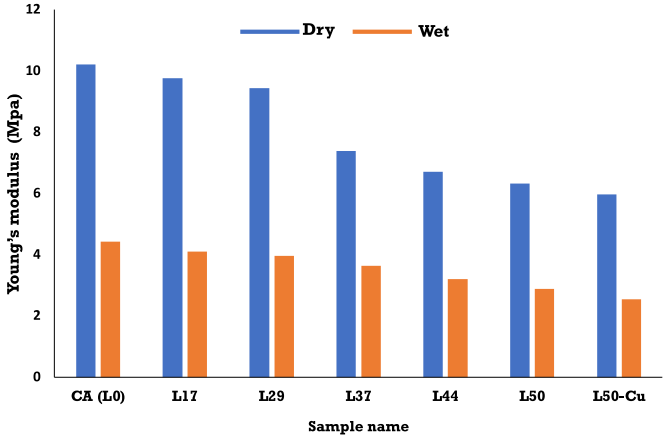

Fig. 5. Young's modulus of nanofibrous mats; L0/Cu, L17/Cu, L29/Cu, L37/Cu, and L44/Cu under dry and wet conditions (immersed in distilled water for 24 h).

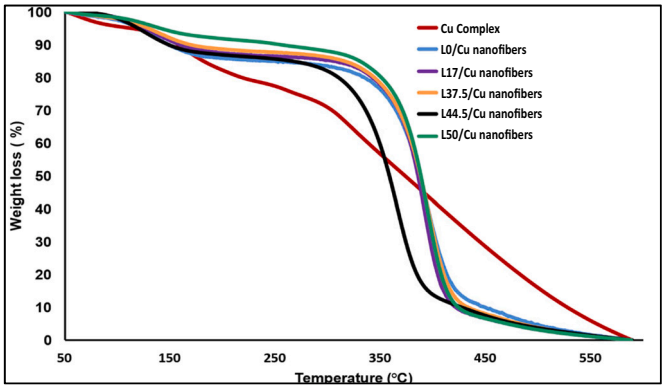

Fig. 6. TGA of Cu complex loaded CA/lignin nanofibers.

Table 3
Bactericidal action and width of ZOI of five explored compounds towards skin bacterial pathogenic lineages.

Explored compounds	Diffusion assays	Targeted pathogenic bacteria			
		P. aeruginosa	*A. baumannii*	*S. epidermidis*	*S. faecalis*
Cu-Br	Disc	17 ± 0.11	15 ± 0.21	10 ± 0.10	12 ± 0.10
	Well	19 ± 0.25	17 ± 0.14	12 ± 0.15	15 ± 0.15
Cu-tolyl	Disc	14 ± 0.21	13 ± 0.23	8 ± 0.24	10 ± 0.24
	Well	16 ± 0.16	15 ± 0.20	11 ± 0.11	13 ± 0.11
Cu-Cl	Disc	No zone	No zone	No zone	No zone
	Well	No zone	No zone	No zone	No zone
Cu-tetrahydro	Disc	21 ± 0.18	19 ± 0.25	14 ± 0.15	16 ± 0.15
	Well	23 ± 0.22	20 ± 0.18	15 ± 0.24	18 ± 0.24
Cu-amine	Disc	25 ± 0.19	22 ± 0.12	18 ± 0.21	20 ± 0.18
	Well	27 ± 0.21	24 ± 0.16	20 ± 0.17	22 ± 0.17
Ampicillin	Disc	15 ± 0.15	16 ± 0.17	13 ± 0.20	14 ± 0.10
	Well	17 ± 0.13	18 ± 0.21	15 ± 0.14	16 ± 0.21

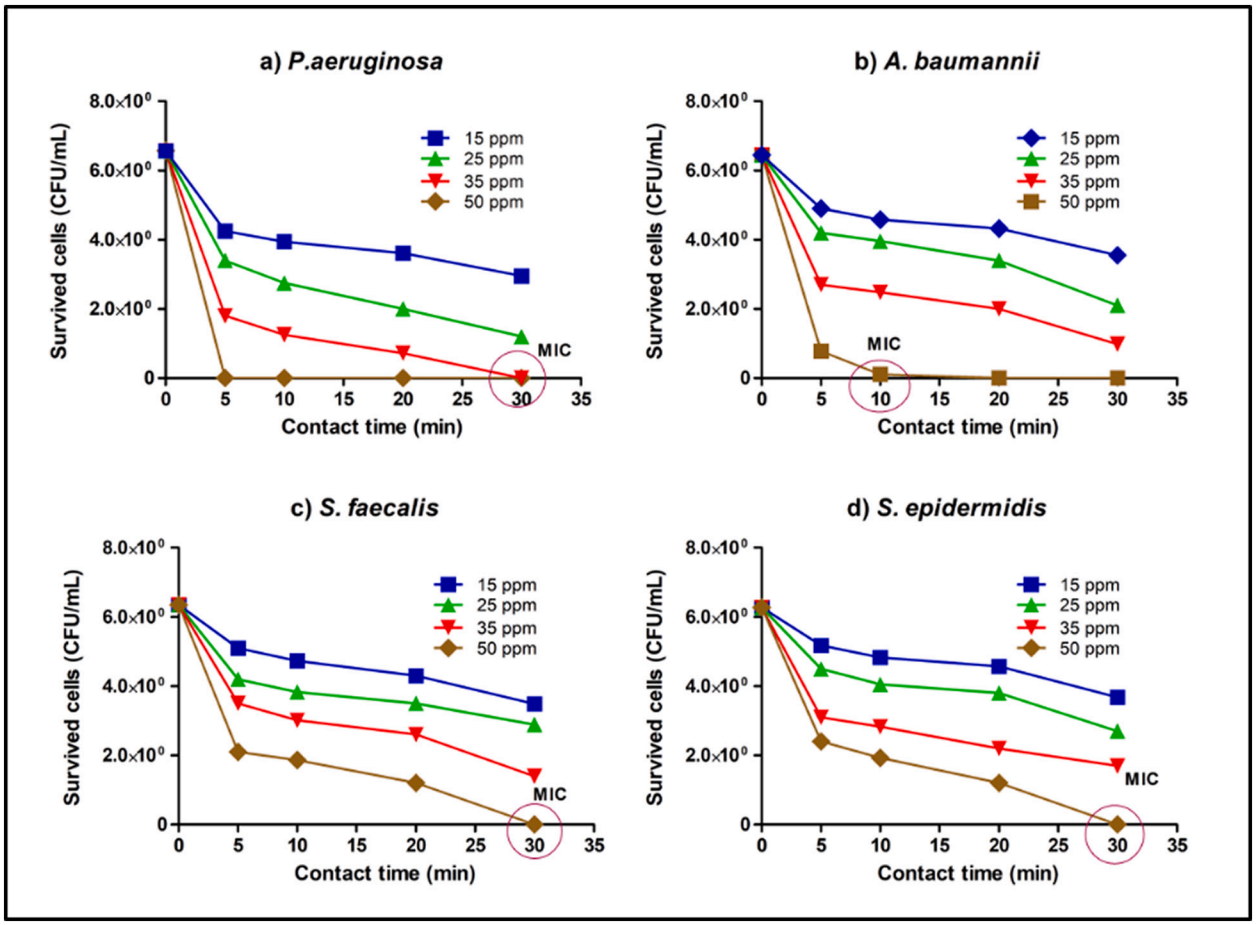

Fig. 7. MIC values of complexed Cu—Br compound against a) *P. aeruginosa*, b) *A. baumannii*, c) *S. faecalis*, and d) *S. epidermidis*.

2.11. Mechanical properties: tensile strength

The tensile strength properties were measured with a mechanical tester (Instron-USA). Nanofiber mats were cut into identical pieces (2 cm × 6 cm) with a thickness of 0.20 mm. Two grips held the sample, and the extension force was applied (3 mm/min), and the stress-strain curve was recorded. The same test was performed but used wet samples. The nanofiber mats were soaked in urine solution 24 h before measurement. It is critical to measure the elastic modulus of the nanofiber mats since it is going to be used in diapers. The structure of the nanofibers is expected to deform after absorbing urine under pressure. Therefore, the elastic modulus indicates the mat's stiffness, which relates to the fabric's comfort.

2.12. Evaluation of the biological activity

Five skin pathogenic bacterial lineages such as *Pseudomonas aeruginosa*, *Acinetobacter baumannii*, *Staphylococcus epidermidis*, and *Streptococcus faecalis* were used in this study. After that, 100 μl of preserved bacteria were cultivated into tubes containing 25 mL of Tryptic Soya broth (TSB), and the seeded tubes were stored in the incubator for 24 h at 37 °C. After the incubation in the ideal environment, each tube was centrifuged at 5000 rpm for 15 min, and the cells-containing pellet was extruded and purified by washing three times with phosphate-buffered saline (PBS) to exclude any undesirable particles. Log count 6 CFU/mL was the density of intended bacteria.

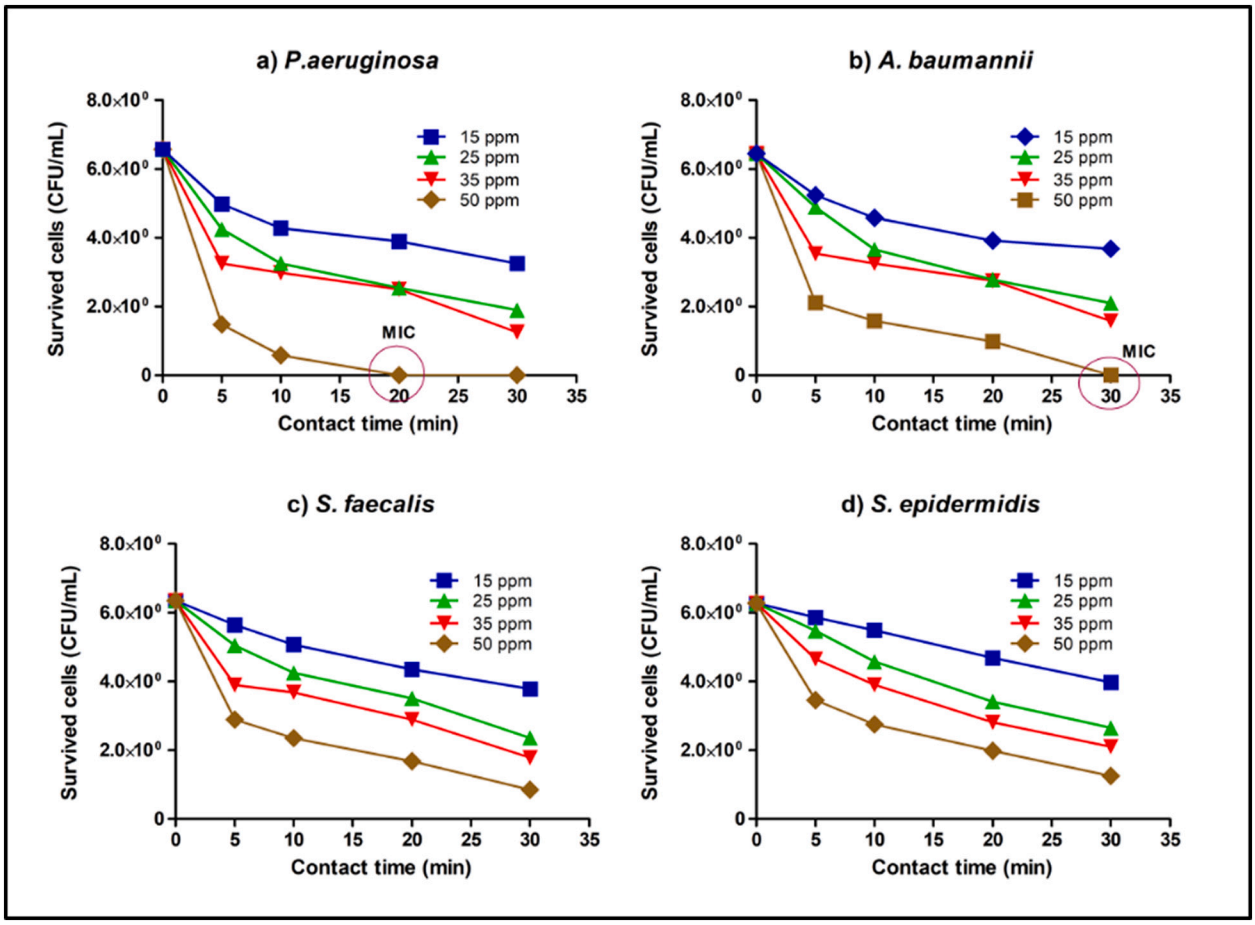

Fig. 8. MIC values of complexed Cu-tolyl compound against a) *P. aeruginosa*, b) *A. baumannii*, c) *S. faecalis*, and d) *S. epidermidis*.

2.12.1. Inhibition zone test

The bactericidal potential of five explored synthesized complexed compounds (Cu-Br, Cu-toyl, Cu-Cl, Cu-tetrahydro, and Cu-amine) was investigated against the mentioned above bacterial lineages using both disc and well diffusion techniques as previously described [37]. A hundred μl of bacterial suspension was appropriately disseminated on the surface of Mueller–Hinton agar (MHA) medium. In disc diffusion assay, sterile filter paper discs (8 mm in diameter) were filled with a volume (50 μl) of stock solution of each synthesized complexed compound. Then, impregnated discs were placed onto the surface of the MHA medium. However, the same volume of each nanomaterial was poured into the well, punched in the deep layer of the MHA agar medium. After that, all prepared plates were maintained in the incubator for 18-24 h at 37 °C. The respective zones of inhibition around individual discs were measured using a Vernier caliper.

2.12.2. Cell viability estimation

The microdilution method was employed to appraise the minimum inhibitory concentration (MIC) values and populations of cell viability communities for each nanomaterial studied. First, a suitable proportion of bacterial culture suspension with a log10 of 6.42 CFU/mL concentration was conveyed into tubes with 10 mL sterile water. Then, various concentrations (15, 25, 35, and 50 ppm) of explored synthesized complex compounds were injected into the infected tubes [37]. Finally, the quantities of remaining colony-forming units after exposure to explored nanomaterials were quantified using plate count viability assay at various exposure times (0, 5, 15, and 30 min) and contrasted to a positive control (suspension lack of nanoclusters) to assess the bactericidal tendency [38].

2.12.3. Assessment of physiological evolution

Physiological variability in the targeted bacterial evolution was intensely investigated by estimating the growth curve and liberated intercellular protein.

2.12.4. Growth kinetic analysis

One hundred μl of the bacterial cell suspension was introduced into two tubes containing 50 mL sterile Trypticase Soy broth medium (TBS). One of these tubes contained effective concentrations of the synthesized complex compounds (50 ppm), whereas another tube without the nanocomposite served as a negative control. Under particular circumstances, all tubes were located in a shaking incubator (at 37 °C and 200 rpm of stirring). After that, the respective samples were taken periodically every 2 h through a whole day (n = 12 values) to be investigated [38].

The potential of bacterial reproduction and expanding bacterial cell populations were examined. Experimental works were conducted by estimating the cell populations in the obtained sample (1 mL). The optical densities of collected samples were estimated spectrophotometrically at 600 nm before and after treatment with the effective dose of each explored nanocomposite [39].

2.12.5. Measuring the amount of leakage protein

Evaluation of the concentration of leakage protein, which is the outflow of cell contents, was applied as an indicator of the destruction of the bacterial cell membrane structure. The amount of protein released from damaged bacterial cells was appraised using the Coomassie blue technique [40].

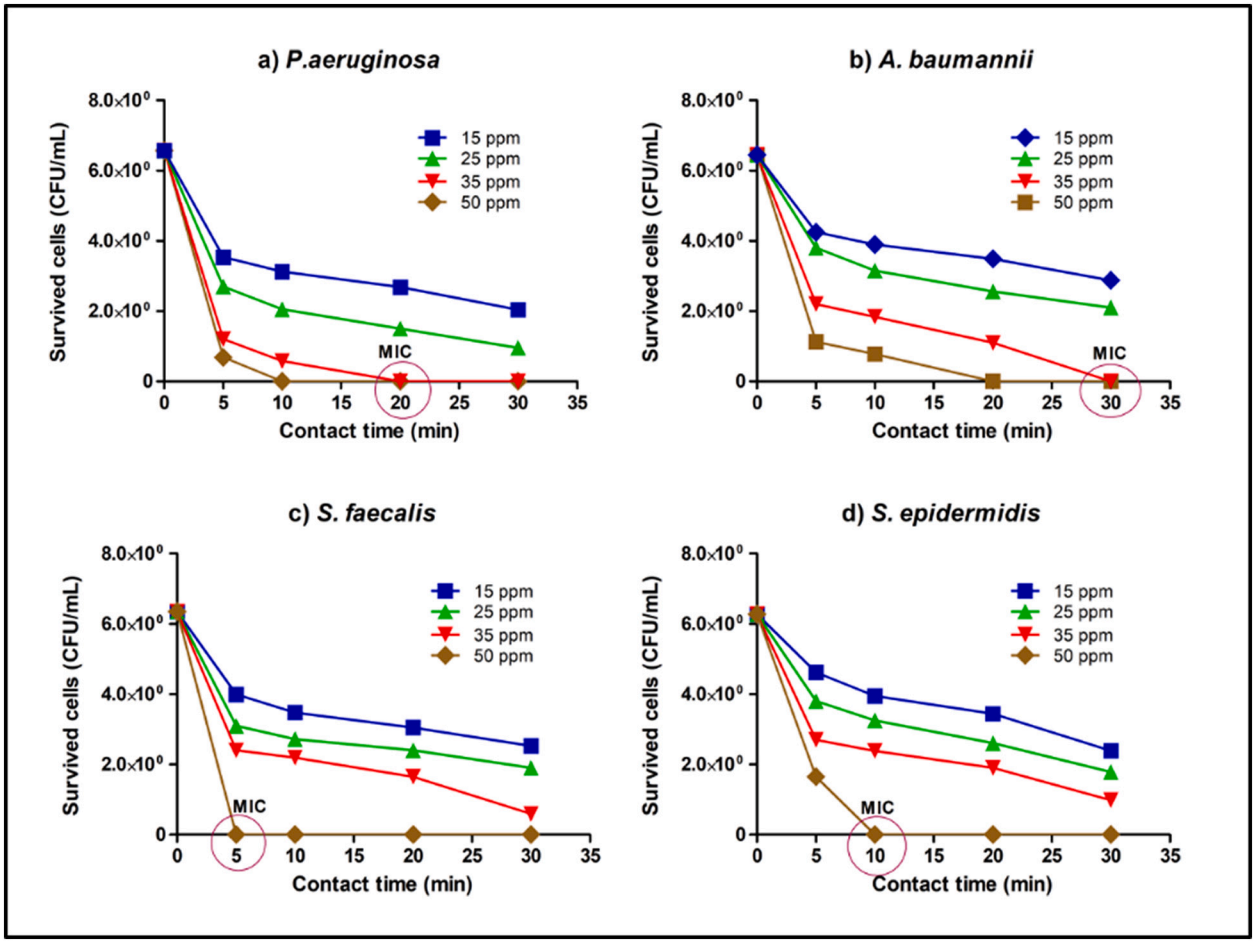

Fig. 9. MIC values of complexed Cu tetrahydrate compound against a) *P. aeruginosa*, b) *A. baumannii*, c) *S. faecalis*, and d) *S. epidermidis*.

2.12.6. Biocompatibility and toxicity assay

The toxicological properties of the synthesized complex compounds for establishing their biocompatibility were performed using a Microtox® Model 500 (M500) Analyzer (Modern Water Inc., New Castle, DE, USA) to guarantee their reliability and safety use in biomedical applications without inflicting injured or harmful impacts on humankind. The cytotoxicity of the examined substances was measured at the highest dose concentration (100 ppm) [37].

2.12.7. Biological evaluation of electrospun nanofibers

Based on the morphological characterization of five types of electrospun nanofibers, CA electrospun nanofibers were selected to be posteriorly loaded with three different doses of the remarkable antibacterial Cu + amin complexed compounds (L50, L1, L2, and L3). A swatch of new electrospun nanofibers was cut into pieces (2 × 2 cm). The antibacterial potential of each electrospun nanofiber was evaluated, as mentioned previously.

2.12.8. Bioburden assay of electrospun nanofibers

Electrospun nanofibers swatches were immersed into tubes containing 10 mL PBS, and then each tube was injected with 25 μl of each bacterial culture suspension and preserved at 30 °C and 80% relative humidity. Immediately the following inoculation at 1, 3, and 6 days of incubation, the number of surviving bacterial cells in PBS solution was enumerated. Further, the bacterial adhesion and biofilm formation over each swatch was evaluated according to the previous published work [41].

3. Results and discussion

The ultimate goal of this study is to develop an efficient antimicrobial layer from biobased and sustainable sources (cellulose acetate and lignin) appropriate for diaper applications. The antibacterial properties were acquired via incorporating a newly synthesized copper complex to control diaper dermatitis. In addition, we aimed at valorizing and adding value to lignin by integrating it in high added value products like medicated diapers. Therefore, we studied the effect of lignin concentration on the physical properties of the formed nanofibers using FESEM, TGA, tensile strength, water absorbency, and contact angle techniques to provide valuable insight into the behavior of lignin concerning other fiber spinning processes.

3.1. Chemical characterization of Schiff bases and their respective Cu(II) complexes

Characterization of the obtained Schiff base was proved using FTIR, ^{1}HNMR, and Mass Spectrometry. The data is presented in Figs. S1–S5 in the Supplementary document.

3.1.1. 2-Methoxy-4-((thiazol-2-ylimino)methyl)phenol

Brown precipitate, yield (85%), FTIR, cm^{-1}: 682 (C—S), 860 (C—Cl), 1450 (C═C, Ar.), 1597 (C═N, thiazole ring), 1666 (C═N, azomethine), 2990 (C—H stretching, aliphatic), 3280 (C—H, stretching, Ar.), 3317 (O—H stretching). ^{1}H NMR (300 MHz, DMSO) δ = 7.87 (s, 1H, OH), 6.05 (s, 1H, CH═N), 5.81 (s, 1H), 5.59–5.44 (m, 3H), 4.33 (s, 1H), 2.15 (s, 3H). ESI-MS, purity: 98%. LC-MS (m/z) exact mass: cal. 234.27, found 233.76 [M−H]$^{-}$.

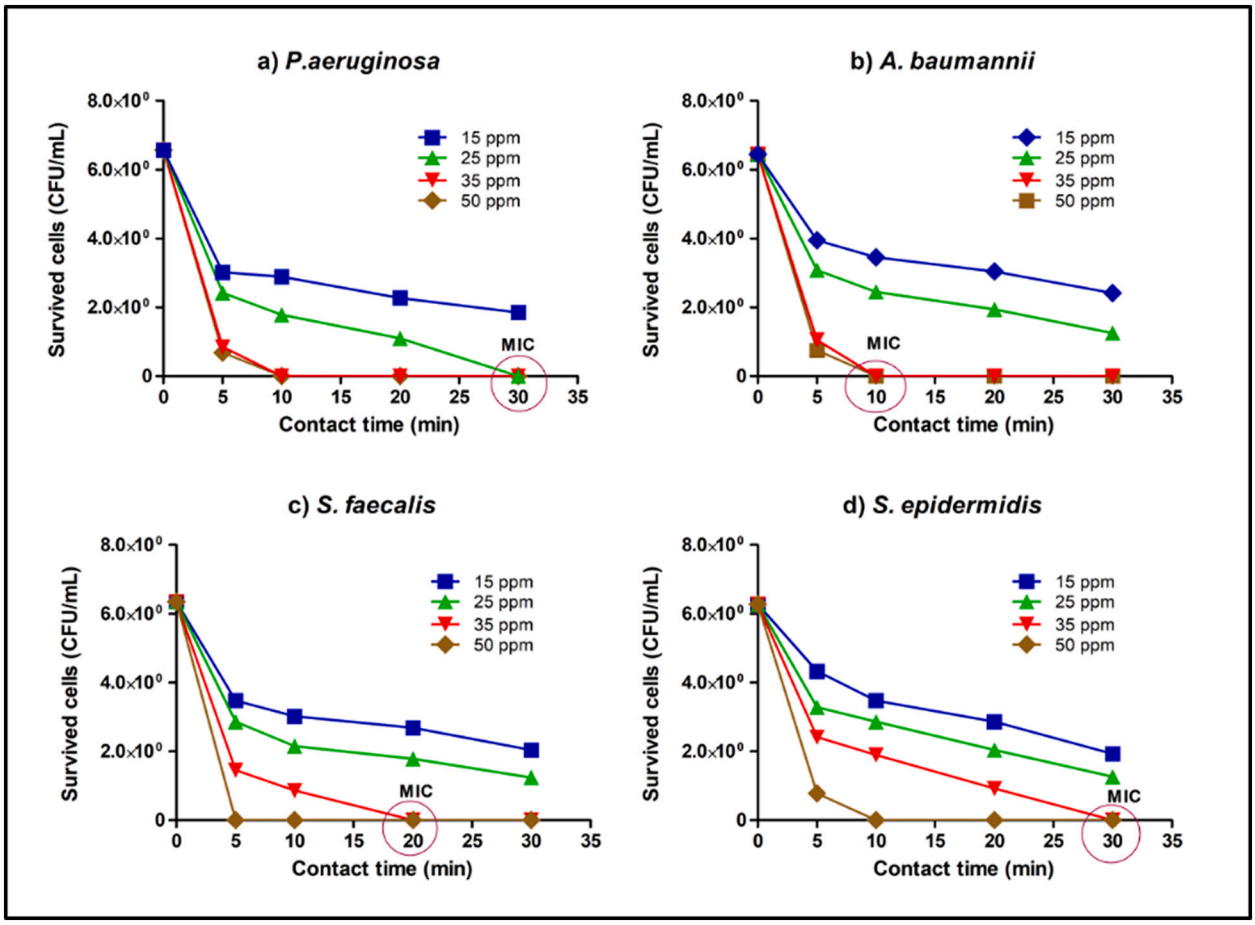

Fig. 10. MIC values of complexed Cu-amine compound against a) *P. aeruginosa*, b) *A. baumannii*, c) *S. faecalis*, and d) *S. epidermidis*.

3.1.2. 4-(((4-(4-Chlorophenyl)thiazol-2-yl)imino)methyl)-2-methoxyphenol

Green precipitate, yield (87%), FTIR, cm^{-1}: 643 (C—S), 830 (C—Cl), 1421 (C═C, Ar.), 1529 (C═N, thiazole ring), 1617 (C═N, azomethine), 2988 (C—H stretching, aliphatic), 3279 (C—H, stretching, Ar.), 3426 (O—H stretching). ^{1}H NMR (300 MHz, DMSO) δ = 9.31 (s, 1H, OH), 8.94 (s, 1H, CH═N), 8.50–7.75 (m, 1H), 6.75–5.55 (m, 4H), 4.90 (s, 1H), 4.68 (s, 2H), 1.66 (s, 3H, OCH_3). LC-MS, purity: 98%. LC-MS (*m/z*) exact mass: cal. 344.81, found 345.0 $[M+H]^+$.

3.1.3. 4-(((4-(4-Bromophenyl)thiazol-2-yl)imino)methyl)-2-methoxyphenol

Green precipitate, yield (89%), FTIR, cm^{-1}: 632 (C—S), 725 (C—Br), 1428 (C═C, Ar.), 1588 (C═N, thiazole ring), 1671 (C═N, azomethine), 2963 (C—H stretching, aliphatic), 3280 (C—H, stretching, Ar.), 3329 (O—H stretching). ^{1}H NMR (300 MHz, DMSO) δ = 8.58 (s, 1H, OH), 7.66 (s, 1H, CH═N), 6.64–5.29 (m, 5H), 4.55 (s, 1H), 4.34 (s, 2H), 1.31 (s, 3H, OCH_3). ESI-MS, purity: 98%. LC-MS (*m/z*) exact mass: cal. 389.27, found 390.09 $[M+H]^+$.

3.1.4. 2-Methoxy-4-(((4-(p-tolyl)thiazol-2-yl)imino)methyl)phenol

Green precipitate, yield (87%), FTIR, cm^{-1}: 633 (C—S), 1459 (C═C, Ar.), 1588 (C═N, thiazole ring), 1670 (C═N, azomethine), 2980 (C—H stretching, aliphatic), 3182 (C—H, stretching, Ar.), 3323 (O—H stretching). ^{1}H NMR (300 MHz, DMSO) δ = 8.60 (s, 1H, OH), 7.69 (s, 1H, CH═N), 6.62–5.27 (m, 5H), 4.59 (s, 1H), 4.40 (s, 2H), 1.07 (s, 3H, OCH_3), 0.74 (s, 3H, CH_3). ESI-MS, purity: 98%. LC-MS (m/z) exact mass: cal. 324.40, found 323.09 $[M-H]^-$.

3.1.5. 2-Methoxy-4-(((4-(5,6,7,8-tetrahydronaphthalen-2-yl)thiazol-2-yl)imino)methyl)phenol

Green precipitate, yield (87%), FTIR (KBr), cm^{-1}: 633 (C—S), 1428 (C═C, Ar.), 1587 (C═N, thiazole ring), 1672 (C═N, azomethine), 2927 (C—H stretching, aliphatic), 3266 (C—H, stretching, Ar.), 3321 (O—H stretching). ^{1}H NMR (300 MHz, DMSO) δ = 8.56 (s, 1H, OH), 7.64 (s, 1H, CH═N), 6.51–5.96 (m, 1H), 6.06–5.22 (m, 3H), 4.55 (s, 1H), 4.39 (s, 2H), 2.15 (s, 3H, OCH_3), 1.65–0.14 (m, 8H, $4CH_2$). ESI-MS, purity: 98%. LC-MS (*m/z*) exact mass: cal. 364.46, found 363.12 $[M-H]^-$.

Characterization of the final copper complexes was proved using FTIR. The data is presented in Figs. S6–S10 in the Supplementary document. The obtained yield of the copper complexes is presented in Table 2.

In the coordination of the metal (Cu) to the Schiff base through the nitrogen atom of the azomethine, a reduction in the electron intensity of the azomethine band is expected. It is noticed that a shift of the vibration characteristic of azomethine ν(C═N) to lower frequencies in Cu-amine, Cu—Cl, Cu—Br, Cu-tolyl, and Cu-tetrahydro by 3, 14, 4, 2, and 2, respectively, compared to the ligands [42]. Additionally, the intensity of ν(C═N) peaks decreased in all the complexes compared to the ligands. On the other hand, a shift of the complexes' ring ν(C═N) vibration characteristic compared to the ligands is noticed. This indicates the metal's coordination to ligand by azomethine nitrogen and ring nitrogen [43].

3.2. Morphology of cellulose acetate/lignin nanofiber mats

The surface topography of nanofibers from CA and CA/lig nanocomposite is shown in Fig. 1. The samples labeled a, b, c, d, e, and f are

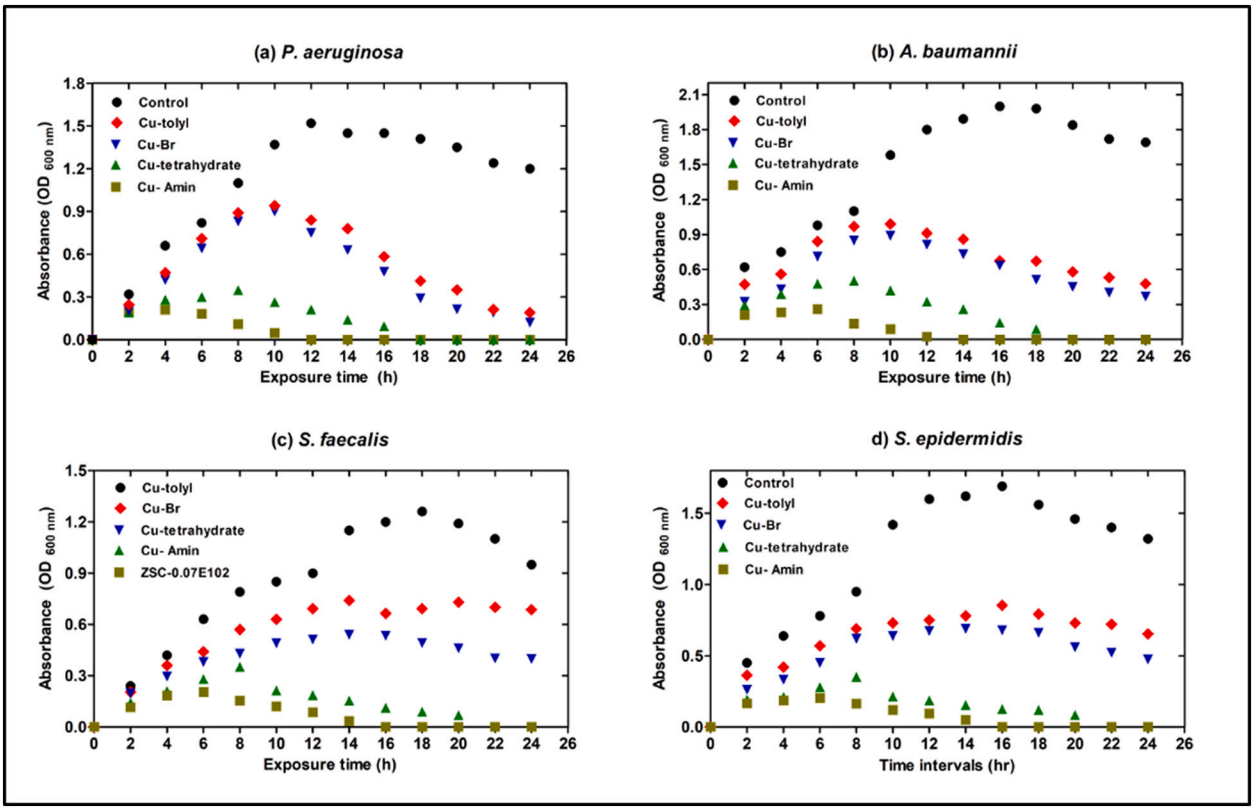

Fig. 11. Growth curves of a) *P. aeruginosa*, b) *A. baumannii*, c) *S. faecalis*, d) *S. epidermidis* cultured in TSB broth with effective concentrations (50 ppm) of four explored compounds.

imaged for the surface morphology Fig. 1-a shows the morphological structure of CA (zero lignin content, L0) nanofibers. It is clear that the surface is smooth however, there are some irregular shaped fibers. The average diameter was 250 nm (±20). The images of as-obtained nanofibers using different lignin content (L17, L29, L37, L44, and L50) are presented in Fig. 1 and coded as b, c, d, e, and f, respectively. The images reveal that the nanofibers clearly are smooth, uniform, and beads-free with increased diameter. The average diameters were found to be 280 nm (±25), 310 nm (±35), 350 nm (±20), 410 nm (±35), and 450 nm (±20) for L17, L29, L37, L44, and L50, respectively. These results suggest that incorporating lignin led to increments in fiber diameter, but more homogeneity was noticed. This could be attributed to the higher conductivity of lignin solutions gained from their sulfonate content.

3.2.1. *Morphology of cellulose acetate/lignin fiber mats loaded with Cu (II) complex*

Sample L50 was selected for the drug loading experiment. The SEM technique was employed to clarify the effect of the Cu complex on the spinnability and morphology of the nanofibers. The anticipated active antimicrobial material, Cu (II)-amine complex, was added to the CA/Lig spinning solutions (0.5% wt/v). After complete dissolution of the Cu complex, the resulting solutions were electrospun, and its SEM micrograph is presented in Fig. 2-a. Evidently, the drug-loaded fibers were found to be smooth. Since neither drug crystals nor aggregates are observed on the surfaces of the fibers, it is concluded that the drug is well encapsulated within the fibers. The SEM also clearly shows that incorporating Cu complex in the electrospun CA and CA/lignin fibers mats does not exert any remarkable change in the fiber morphology. The nanofibers were submitted to further characterization using Energy Dispersive X-ray (EDX). The elemental analysis of this EDX was imaged in Fig. 2-b. It is worth mentioning that sulfonate-lignin was sued in this experiment so that sulfur content could be used as an indicator of lignin presence. As is evident from the element mapping, carbon and oxygen are predominant in the mats followed by sulfur and copper. Fig. 2-c shows the smooth surface of the nanofiber at high magnification. The cross-section of the fibers is presented in Fig. 2-d and e at higher magnification. The fibers look intact with perfect cylindrical shape. However, there are some irregularities onside the fiber which suggests the presence of some degree of phase separation between cellulose acetate and lignin polymers.

3.3. *Change in hydrophilicity: water contact angle*

For hygienic articles, both hydrophilicity and water retention under pressure is desired. Cellulose acetate possesses good water retention under pressure; however, lower hydrophilicity than cellulose. However, the size of the fibers plays an essential role in fluid absorbency. In addition, lignin was incorporated in the current matrices to improve the hydrophilicity and accelerate the biodegradability of the nanofibers. The surface contact angle can be used to refer to the wettability of the as-prepared nanofiber mats and was measured using sessile drop observation [44]. The water droplet formed on the CA nanofibers (L0) is shown in Fig. 3-A. The surface contact angle of the CA nanofiber displays a value as high as 81° due to the partial hydrophobic nature of acetyl groups in the molecular structure of cellulose acetate. However, it is lower than other numbers reported in the literature (102°) due to the small size of the fibers (nanometer range) and the high porosity and surface area of the fiber mat [45]. Fig. 3-B shows a significant decrease in the contact angle (73°) on CA/lignin nanofibers at the lowest concentration of lignin (L17), which may be ascribed to the presence of hydrophilic sulfonate groups located on lignin structure. A similar effect was observed upon increasing the lignin content. Fig. 2-c, d, and e shows a dramatic drop in the contact angle value of 45°, 30°, and 8° for L29, L37, and L44, respectively. Concerning sample (L50), no angles were detected to the high wettability of the surface. Therefore, L50 was chosen for Cu-complex loading and used in further analysis.

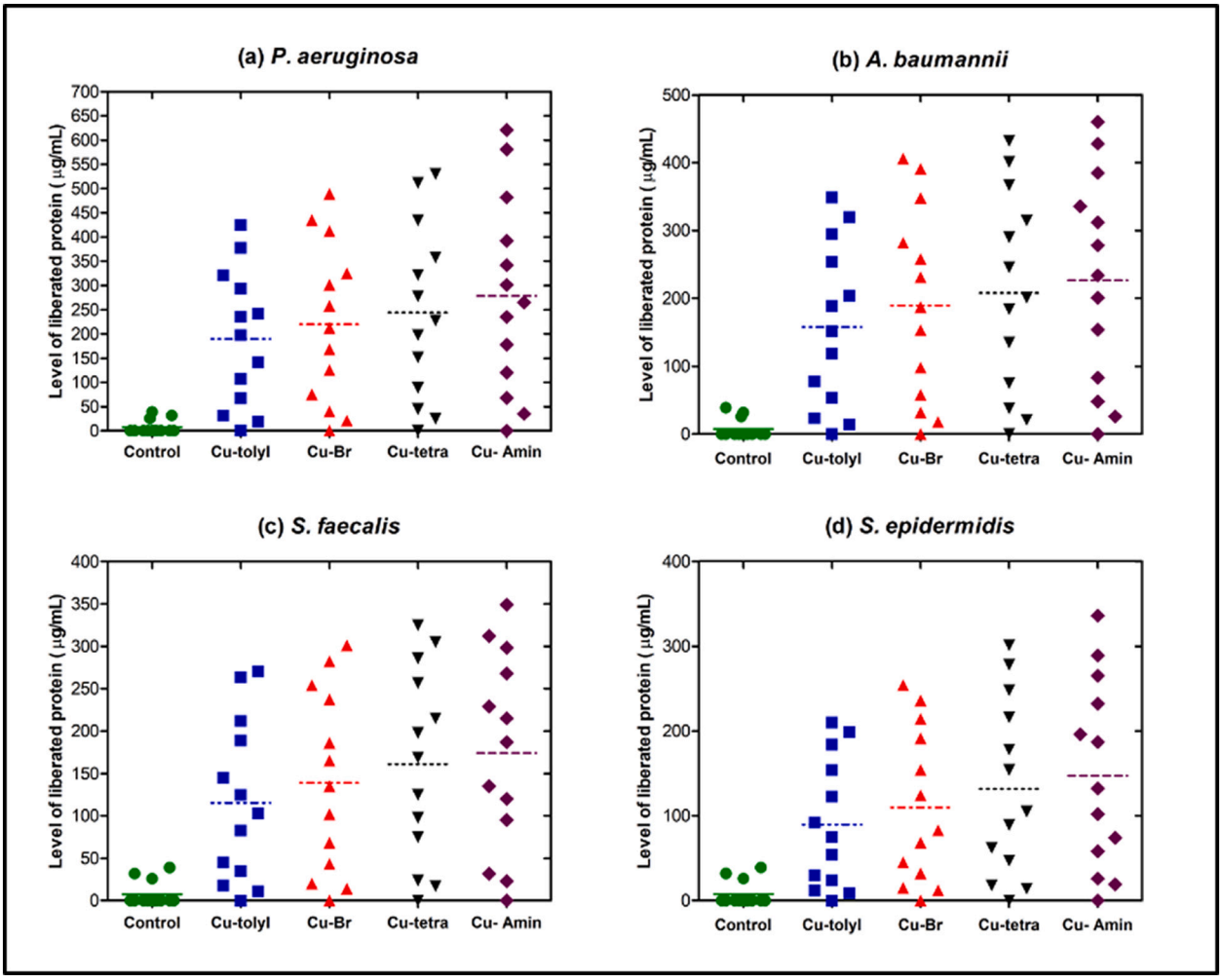

Fig. 12. Amounts of liberated intracellular protein of a) *P. aeruginosa*, b) *A. baumannii*, c) *S. faecalis*, d) *S. epidermidis* cultured in TSB broth with effective concentrations (50 ppm) of four explored compounds.

Table 4
Concentrations Microtox® EC50% of the 500 mg/L as MICs of Cu-complexes.

Studied nanofibers	EC_{50}% concentrations			References of toxic ranges	
	5 min	10 min	15 min	EC_{50}% degree	Toxicity level
Cu-Br	325	318	291	0–19	Extremely toxic
Cu-tolyl	308	292	273	20–39	Very toxic
Cu-tetrahydrate	313	305	285	40–59	Toxic
Cu-amine	294	254	224	60–79	Mild toxic
				≥100	Non-toxic and safe

Table 5
The diameters of ZOI (mm) of explored polymers around DD-causing bacteria.

Fabricated electrospun nanofibers	Targeted pathogenic bacteria			
	P. aeruginosa	*A. baumannii*	*S. epidermidis*	*S. faecalis*
L50	NZ	NZ	NZ	NZ
L50-1	14 ± 0.24	12 ± 0.13	8 ± 0.21	10 ± 0.18
L50-2	17 ± 0.15	15 ± 0.21	11 ± 0.14	13 ± 0.21
L50-3	18 ± 0.20	15 ± 0.18	11 ± 0.21	13 ± 0.18

NZ = no-zone.

3.4. Equilibrium absorbency and absorbency under load

Since the current cellulose acetate/lignin nanofibers will be integrated into the hygienic articles' absorption core, its absorption capacity should be estimated. Therefore, the absorption at equilibrium (after 24 h) and under load in urine solution was estimated for the electrospun CA/Lig nanofibers and presented in Fig. 4. Fig. 4-A shows the change in the color associated with increasing lignin content. Furthermore, it shows that the nanofiber mats are wet stable, do not disintegrate, and stay intact after 24 h. Fig. 4-B shows the change in color from white to pale yellow to brownish due to the incorporation of lignin and Cu-complex. Generally, the color of the nanofibers gets darker upon wetting. In addition, Fig. 4-B shows the values of nanofiber absorbency at equilibrium and under load. CA nanofibers were able to absorb urine 2300% of its dry weight. The absorption capacity increased by increasing the lignin content in the nanofibers by 13%, 28%, 47%, 67%, and 80% for L17, L29, L37, L44, and L50, respectively. Again, this significant increase in absorbency could be attributed to the sulfonate groups present in lignin. Such results are in agreement with the water contact angle data. The obtained results are significantly higher than those reported by Sharma et al. [16] for pure cellulose acetate nanofibers. The copper complex loaded sample (L50-Cu complex) showed a marginal decrease of 6% compared with its drug-free counterpart, L50, which may be attributed to the hydrophobic nature of the loaded copper complex.

The swelling under load (Fig. 4-C) test measures the effect of

Table 6
Survival of microorganisms and bacterial adhesion on fabricated electrospun nanofibers stored at 80% relative humidity and 30 °C after 1 day of incubation.

Fabricated electrospun nanofibers	Electrospun nanofibers							
	L50		L50-1		L50-2		L50-3	
	Planktonic cells	Biofilm cells	Planktonic cells	Biofilm cells	Planktonic cells	Biofilm cells	Planktonic cells	Biofilm cells
P. aeruginosa	6.24	1.5	5.41	n.d.	5.04	n.g.	5.01	n.g.
A. baumannii	6.35	1.1	6.35	n.d.	5.48	n.g.	5.22	n.g.
S. epidermidis	6.85	0.78	6.85	n.d.	5.95	n.g.	5.83	n.g.
S. faecalis	6.48	0.95	6.48	n.d.	5.52	n.g.	5.46	n.g.

n.g. = no growth.

Table 7
Survival of microorganisms and bacterial adhesion on fabricated electrospun nanofibers stored at 80% relative humidity and 30 °C after 3 days of incubation.

Fabricated electrospun nanofibers	electrospun nanofibers							
	L50		L50-1		L50-2		L50-3	
	Planktonic cells	Biofilm cells	Planktonic cells	Biofilm cells	Planktonic cells	Biofilm cells	Planktonic cells	Biofilm cells
P. aeruginosa	6.24	2.2	4.11	0.48	3.89	n.g.	3.81	n.g.
A. baumannii	6.35	1.68	4.72	0.61	4.12	n.g.	4.08	n.g.
S. epidermidis	6.85	1.23	5.1	0.72	4.75	n.g.	4.63	n.g.
S. faecalis	6.48	1.45	4.85	0.85	4.35	n.g.	4.24	n.g.

Table 8
Survival of microorganisms and bacterial adhesion on fabricated electrospun nanofibers stored at 80% relative humidity and 30 °C after 6 days of incubation.

Fabricated electrospun nanofibers	Electrospun nanofibers							
	L50		L50-1		L50-2		L50-3	
	Planktonic cells	Biofilm cells	Planktonic cells	Biofilm cells	Planktonic cells	Biofilm cells	Planktonic cells	Biofilm cells
P. aeruginosa	6.24	3.8	3.58	0.53	3.14	n.g.	3.11	n.g.
A. baumannii	6.35	3.47	4.21	0.75	3.56	n.g.	3.48	n.g.
S. epidermidis	6.85	2.48	4.83	0.83	4.25	n.g.	4.21	n.g.
S. faecalis	6.48	2.98	4.49	0.99	3.84	n.g.	3.78	n.g.

n.g. = no growth.

mechanical compression on the swelling process of the sample. This test is crucial since the proposed application (absorbing diapers). In addition, the nanofiber mats' surface properties and internal structure may change by applying compressive load. As expected, the absorbance capacity of the nanofiber mats was lower when tested under load. For pure CA, the absorbency percentage was 1300% of its dry weight and 54% lower than its free absorbency value. On the other hand, the absorbency of lignin-containing samples increased by increasing the lignin content. As a result, samples L17, L29, L37, L44, and L50 were 55, 39, 25, and 27% lower than free swollen counterparts.

3.5. Mechanical properties: tensile strength

The absorbent core's inadequate tensile strength may cause it to break or tear, resulting in fluid leakage and limiting the product's efficiency. Consequently, the mechanical performance of electrospun nanofibers (elastic modulus in dry and wet environments) was assessed, and the findings are shown in Fig. 5. The modulus of elasticity was calculated using the original stress-strain data. The elastic modulus of electrospun nanofibers samples differs significantly.

CA (L0), L17, L29, L37, L44, L50, and L50/Cu have moduli of 10.21, 9.76, 9.44, 7.39, 6.72, 6.32, and 5.98 MPa, respectively, in dry conditions. On the other hand, the elasticity modulus of L44, L50, and L50/Cu do not change significantly. The values of the wet samples, CA (L0), L17, L29, L37, L44, L50, and L50/Cu, showed that the elastic modulus was significantly reduced yet with good mechanical properties. These findings agree with other results in the literature [30,32,46] suggest that CA nanofibers loaded with lignin and Cu complex can be employed in the absorbent core in hygiene products due to their adequate mechanical strength compared with the commercialized cellulose acetate nanofibers.

3.6. Thermal properties of the nanofiber mats

The thermal behavior of Cu complex and Cu complex loaded CA/lignin nanofibers are evaluated using TGA, and the obtained data are displayed in Fig. 6. It is observed that Cu(II) complex decomposes mainly in two steps. The first step is water evaporation, as depicted by the peak at 90 °C. Then, the complex further decomposes in the second step in the range of 270–340 °C with weight loss of more than 40% associated with partial loss of complex weight. The weight loss percent is sharply decreased upon increasing the temperature and reaching 80% at 450 °C.

On the other hand, in CA/lignin fibers, water evaporation occurs at 85–100 °C. The second thermal degradation of CA/lignin using different ratios of lignin (20, 40, 60%) appears at 370 °C with a weight loss of around 20%. Increasing the lignin concentration to 80% accelerates the thermal degradation of the resulting CA/lignin/Cu complex nanofibers, which may be attributed to the plasticization interaction effect of lignin and cellulose acetate [47,48]. The obtained data agrees with the earlier data of contact angle and wicking measurements. From the above data, the thermal stability of the Cu-complex was enhanced by blending with CA/lignin solutions prior to electrospinning and confirmed that Lignin and CA could act as carrying and stabilizing agents for Cu complex against degradation.

3.7. Evaluation of biological activity

3.7.1. Bactericidal action of explored compounds

The infection of diaper dermatitis-causing pathogenic

microorganisms has become a significant obstacle in the medical and the pharmaceutical sectors since they are challenging to manipulate with presently offered marketed medications. Switchover metal binding complexes have been extensively researched for their bactericidal, fungicide, and cytotoxic chemotherapeutic capabilities. It has been examined against various harmful fungi and bacteria, and the results have been encouraging. Five complex compounds were successfully fabricated to overcome the drawback of the antibiotics. Bactericidal activity of these fabricated nanoclusters was performed against four pathogenic bacterial (*P. aeruginosa*, *A. baumannii*, *S. epidermidis*, and *S. faecalis*). The verified results of the agar diffusion assay are presented in Table 3. Results exhibited that the highest ZOI was found for Cu Amin against all tested species whose width of ZOI using disc diffusion assay for *P. aeruginosa*, *A. baumannii*, *S. epidermidis*, and *S. faecalis* was 25 ± 0.19, 22 ± 0.12, 18 ± 0.21, and 20 ± 0.18 mm, respectively.

In contrast, results revealed no potential bactericidal impact against all tested bacterial species was documented for Cu—Cl. Besides, the gained results disclosed that *S. epidermidis* as a model of Gram-positive was the most resistant species; but, the most susceptible was *P. aeruginosa* as a model of Gram-positive. Ampicillin was employed as reference antibiotics drugs. This means that Gram-positive species were more resistant to these explored nanoclusters than Gram-negative species. These results are in excellent agreement with those of Ghazy et al. [49] who stated that the rigidity of the cell wall composition of Gram-positive species provides them with the ability to combat the antimicrobial agent. The results could indicate that the complexes of amine and copper groups have a more powerful bactericidal effect against pathogenic bacteria than other complex compounds and use standard antibiotics. The antimicrobial potential of amine groups of the complexes with metals against *B. subtilis*, MRSA, *Ps. aeruginosa*, and *C. albicans* was significantly higher than the standard drug indicating their potentials as antimicrobial agents against these microbes [50].

3.7.2. MIC values and densities of survived cells

Based on the antibacterial screening of five compounds, four (Cu—Br, Cu-tolyl, Cu-tetrahydro, and Cu-amine) were chosen according to their potential antibacterial properties, the MIC values for four screened compounds were assessed against four pathogenic microbial species mentioned above. The initial $\log_{10}$ counts of each targeted bacterial species in the control trial were applied as the corresponding original concentration (6-$\log_{10}$ CFU/mL).

As shown in Fig. 7, the Cu—Br compound's MIC values of 35 ppm within 30 min were recorded against *P. aeruginosa*, and 50 ppm within 20 min was observed for *A. baumannii*. However, the MIC values of *S. epidermidis* and *S. faecalis* were 50 ppm for 30 min. Regarding the Cu-tolyl compound, acquired results revealed that the level of MIC of 50 ppm within 20 and 30 min was recorded for *P. aeruginosa* and *A. baumannii*. In contrast, the highest dose of such compound could not completely inhibit the growth of *S. epidermidis* and *S. faecalis* (Fig. 7). In the case of complexed Cu tetrahydrate, the MIC values were 35 ppm within 20 and 30 min for *P. aeruginosa* and *A. baumannii*. Besides, MIC values of 50 ppm within 5 and 10 min were observed against *S. faecalis* and *S. epidermidis*. In the same context, the MIC values of complexed Cu-amine compound for *P. aeruginosa* were 25 ppm within 30 min. In contrast, 35 ppm within 10, 20, 30 min was reported as MICs values against *A. baumannii*, *S. faecalis*, and *S. epidermidis* (Figs. 8–10).

As a result, the current findings imply that the Cu-amine compound may prevent DD-causing pathogenic microorganisms and hence has the potential to be used in medicine.

3.7.3. Growth kinetics rate

The bactericidal consequence of a therapeutic dose (50 ppm) of explored compounds on the growth curves of the investigated bacterial species is depicted in Fig. 11. While the growth curves of the four target microorganisms were compared before and after exposure to the examined complexed Cu-amine compound, it was observed that the bacteria's growth activity was significantly inhibited and that the organisms were prevented from entering the logarithmic phase of development. Furthermore, all four stages of growth proliferation (lag, log, stationary, and decline phases) for all studied bacterial species were completed within 24 h in the control experiment (without affording adequate doses of compounds). Numerous examinations have explicated that their growth rate is dramatically inhibited when bacteria are treated with Cu nanomaterials [51,52].

3.7.4. Amounts of intracellular protein leakage

One of the physiological chamber indicators in determining the amount of protein produced by damaged bacterial cells. As shown in Fig. 12, the results showed that the amount of pt protein from the targeted bacterial cell upon exposure to the complex Cu-amine was greater than that of the other compounds. The produced protein from untreated bacterial cells reached 39 μg/mL after 24 h. On the other hand, the amounts of liberated intracellular protein increased after exposure to the effective dose (50 ppm) of each compound detected. Moreover, the amounts of intracellular protein released from microbial cells after exposure to the Cu amine complex were the highest. The obtained results agree with El Nahrawy et al. [53] who proved that the amounts of released protein from Gram-negative species are more prominent than from Gram-positive species.

3.7.5. Toxicity test

The results revealed that the EC50 values after 15 min as a prolonged time was 291, 273, 285, and 224 for Cu—Br, Cu-tolyl, Cu-tetrahydrate, and Cu-amine, respectively, implying that all the explored compounds could be employed to inactivate the DD-causing bacterial pathogens without significant hazardous effects to humankind. These results (Table 4) are compatible with Rashdan et al. [54] who confirmed that several created substances had no substantial detrimental consequences. Likewise, the toxicology testing has been investigated by Khalil et al. for a variety of Cu nanocomposites in a series of consecutive works, all of which revealed Cu nanocomposites to be benign [55].

3.7.6. Prospective use of electrospun nanofibers in the diaper

3.7.6.1. Antimicrobial effectiveness testing. Three swatches of electrospun L50 nanofibers were loaded with different effective compounds (Cu-amine complex). To determine the effective loaded doses and the greatest-loaded nanofiber to be applied in diaper manufacturing, the antibacterial activity of all studied nanofibers was conducted against DD-causing bacteria. Results represented in Table 5 revealed that the unloaded electrospun L50 nanofibers had no potential bactericidal action against all tested bacterial species. However, the maximum diameters of zone of inhibition (ZOI) against all targeted bacterial species were found to electrospun nanofibers L50-2 and L50-3, attributed to the significant antibacterial action of loaded materials. In the same context, results noticed that the nanofibers L50-2 and L50-3 had almost the same bactericidal effect.

3.7.6.2. Bioburden investigation. Throughout manufacturing processing and usage by clients, diapers may be polluted with a microbial spectrum. The surveillance of *P. aeruginosa*, *Acinetobacter*, *S. epidermidis*, and *S. faecalis* on diaper swatches stored in infected suspension with tested bacteria under appropriate circumstances to survive for various days was researched to evaluate whether organisms accidentally introduced onto diapers are capable of sustaining and colonizing on the diaper materials to form the microbial biofilm (1, 3, and 6 days). Because of the presence of effective antibacterial agents inside these nanofibers, none of the intended bacterial strains were discovered in L50-2 and L50-3 nanofibers after 6 days, and no biofilm grew over the swatches of nanofibers (Tables 6–8). Unloaded L50 nanofiber, on the other hand, permitted all organisms to adhere after 6 days of storage. As a result of

the lack of antibacterial agents, biofilm could form on the swatches of L50 nanofiber.

Furthermore, the density of bacterial species in each suspension was nearly $\log_{10}$ 6 CFU/mL. The obtained results explicated that the logarithms of all bacterial species were significantly diminished in a solution containing L50-2 and L50-3 nanofibers. The numbers of the initial $\log_{10}$ count of *P. aeruginosa*, *A. baumannii*, *S. epidermidis*, and *S. faecalis* were reduced to 3.11, 3.48, 4.21, and 3.78 CFU/mL, respectively (Tables 6–8).

4. Conclusions

Cellulose acetate (CA) and lignin (Lig) polymers were utilized to produce a medical textile of nanofibrous nature and antibacterial activity for diaper dermatitis (DD) control. The electrospinning technique was successfully employed to produce the nanofibers from the acetone/DMAc solvent system. In addition, lignin improved the spinnability of cellulose acetate and resulted in beads-free mats. Nanofibers with the highest lignin content (L50) showed improved water absorption (4200% increase), surface contact angle (from 81° to 30°) compared with pure CA nanofibers. However, lignin reduced the mechanical strength of the wet mats from 4.5 MP for cellulose acetate to 3.5 MP for CA/Lig-50 (L50).

Antibacterial activity was acquired by loading the newly synthesized aminothiazole copper complex to the nanofibers (L50). A series of copper complexes (five compounds) were prepared, characterized, and thoroughly screened for their antimicrobial activity. All compounds were active against *Pseudomonas aeruginosa*, *Acinetobacter baumannii*, *Staphylococcus epidermidis*, and *Streptococcus faecalis*. However, the most effective compound (Cu-amine) was loaded to the polymeric solutions during electrospinning. The EC50 value after 15 min as a prolonged time was 224 for Cu- amine, implying that it can be used to inactivate the DD-causing bacterial pathogens without significant hazardous effects to humankind. Furthermore, the presence of copper was proved by EDX. The amalgamation of Cu-amino to CA/Lig-50 occurred without any significant change in the surface morphology of the nanofibers but marginally reduced the absorption under load by 6% compared with the unloaded nanofibers. The antibacterial activity of loaded nanofiber mats were investigated by measuring the zone of inhibition and found to be 18 ± 0.20, 15 ± 0.18, 11 ± 0.21, and 13 ± 0.18 for *Pseudomonas aeruginosa*, *Acinetobacter baumannii*, *Staphylococcus epidermidis*, and *Streptococcus faecalis*, respectively. In addition, the bioburden characteristics were investigated. None of the intended bacterial strains were discovered on the nanofibers after six days, and no biofilm grew over the swatches of nanofibers. The release behavior of the Cu-amine complex and hydrophobic drugs in general from CA/Lig systems is still needed to evaluate the system for other applications like wound dressing. Such a study is under investigation by our group. Finally, the obtained results indicate that the tri-component system from CA/Lig/Cu-complex has a promising potential in hygienic products.

CRediT authorship contribution statement

Dalia A. Elsherbiny: Conceptualization, Methodology, Data curation, Validation, Visualization, Writing - Original draft, Writing - Review & editing.
Abdelrahman M. Abdelgawad: Methodology, Data curation, Validation, Visualization, Writing -Original draft, Writing - Review & editing.
Mehrez E. El-Naggar: Methodology, Data curation, Validation, Visualization, Writing - Original draft, Writing - Review & editing.
Bahaa A. Hemdan: Methodology, Data curation, Validation, Visualization, Writing - Original draft, Writing - Review & editing.
Samaneh Ghazanfari and Stefan Jockenhövel: Software, Conceptualization, Conceptualization, Data curation.
Orlando J. Rojas: Supervision, Software, Conceptualization, Conceptualization, Data curation.

Acknowledgements

The authors would like to acknowledge the contribution of the National Research Centre (Egypt) for facilitating antibacterial testing. In addition, our gratitude is extended to Eastman Chemical Company (USA) for providing technical grade cellulose acetate. Furthermore, we would like to thank Mr. Chuck Mooney, the lab manager of the scanning electron microscope at Analytical Instrumentation Facility, North Carolina State University (USA), for helping to image the fiber morphology.

Appendix A. Supplementary data

Supplementary data to this article can be found online at https://doi.org/10.1016/j.ijbiomac.2022.02.192.

References

[1] G.N. Stamatas, C. Zerweck, G. Grove, K.M. Martin, Documentation of impaired epidermal barrier in mild and moderate diaper dermatitis in vivo using noninvasive methods, Pediatr. Dermatol. 28 (2011) 99–107.
[2] M. Šikić Pogačar, U. Maver, N. Marčun Varda, D. Mičetić-Turk, Diagnosis and management of diaper dermatitis in infants with emphasis on skin microbiota in the diaper area, Int. J. Dermatol. 57 (2018) 265–275.
[3] D. Lekan-Rutledge, J. Colling, Urinary incontinence in the frail elderly: even when it's too late to prevent a problem, you can still slow its progress, AJN Am. J. Nurs. 103 (2003) 36–46.
[4] D. Das, Composite nonwovens in absorbent hygiene products, in: Compos. Non-Woven Mater., Elsevier, 2014, pp. 74–88.
[5] S.C. Khoo, X.Y. Phang, C.M. Ng, K.L. Lim, S.S. Lam, N.L. Ma, Recent technologies for treatment and recycling of used disposable baby diapers, Process. Saf. Environ. Prot. 123 (2019) 116–129.
[6] R.A. Burne, Y.-Y.M. Chen, Bacterial ureases in infectious diseases, Microbes Infect. 2 (2000) 533–542.
[7] P.M. de Wet, H. Rode, A. van Dyk, A.J.W. Millar, Perianal candidosis—a comparative study with mupirocin and nystatin, Int. J. Dermatol. 38 (1999) 618–622.
[8] Y. Zheng, Q. Wang, L. Ma, Y. Chen, Y. Gao, G. Zhang, S. Cui, H. Liang, L. Song, C. He, Shifts in the skin microbiome associated with diaper dermatitis and emollient treatment amongst infants and toddlers in China, Exp. Dermatol. 28 (2019) 1289–1297.
[9] W. Cross, R. Cant, D. Manning, S. McCarthy, Addressing information needs of vulnerable communities about incontinence: a survey of ten CALD communities, Collegian. 21 (2014) 209–216.
[10] J.-H. Lin, B.-C. Shiu, C.-W. Lou, Y.-J. Chang, Design and fabrication of smart diapers with antibacterial yarn, J. Healthc. Eng. 2017 (2017).
[11] S.O. Odelhog, Germicidal Absorbent Body, 1983.
[12] J.J. V., Safety of using diapers containing copper oxide in chronic care elderly patients, Open Biol. J. 6 (2013).
[13] H.M. Ahamed, R. Rajendran, C. Balakumar, S. Jayakumar, Prevention of diaper dermatitis in baby diapers with nanoencapsulated natural extracts, in: Proc. 4 Th Int. Conf. Nanostructures, 2012, pp. 12–14.
[14] S.V. Kumar, Sustainable, Microwave Synthesis of Inorganic Nanoparticles and Their Application, 2019.
[15] Y.K. Vaghasiya, R. Nair, M. Soni, S. Baluja, S. Shanda, Synthesis, structural determination and antibacterial activity of compounds derived from vanillin and 4-aminoantipyrine, J. Serbian Chem. Soc. 69 (2004) 991–998.
[16] S.K. Sengupta, O.P. Pandey, B.K. Srivastava, V.K. Sharma, Synthesis, structural and biochemical aspects of titanocene and zirconocene chelates of acetylferrocenyl thiosemicarbazones, Transit. Met. Chem. 23 (1998) 349–353.
[17] V.S. Ashalekshmi, K. Mohanan, Synthesis, characterization and antibacterial activity of copper (II) complexes with N-vanillidene-2-amino-4-phenylthiazole, Asian J. Chem. 20 (2008) 623.
[18] C.P. Barnes, S.A. Sell, E.D. Boland, D.G. Simpson, G.L. Bowlin, Nanofiber technology: designing the next generation of tissue engineering scaffolds, Adv. Drug Deliv. Rev. 59 (2007) 1413–1433.
[19] J. Venugopal, S. Ramakrishna, Applications of polymer nanofibers in biomedicine and biotechnology, Appl. Biochem. Biotechnol. 125 (2005) 147–157.
[20] M.E. Vallejos, M.S. Peresin, O.J. Rojas, All-cellulose composite fibers obtained by electrospinning dispersions of cellulose acetate and cellulose nanocrystals, J. Polym. Environ. 20 (2012) 1075–1083.
[21] K. Jayaraman, M. Kotaki, Y. Zhang, X. Mo, S. Ramakrishna, Recent advances in polymer nanofibers, J. Nanosci. Nanotechnol. 4 (2004) 52–65.
[22] Z.-M. Huang, Y.-Z. Zhang, M. Kotaki, S. Ramakrishna, A review on polymer nanofibers by electrospinning and their applications in nanocomposites, Compos. Sci. Technol. 63 (2003) 2223–2253.
[23] M.E. El-Naggar, A.M. Abdelgawad, C. Salas, O.J. Rojas, Curdlan in fibers as carriers of tetracycline hydrochloride: controlled release and antibacterial activity,

Carbohydr. Polym. 154 (2016) 194–203, https://doi.org/10.1016/j.carbpol.2016.08.042.
[24] A.M. Abdelgawad, M.E. El-Naggar, S.M. Hudson, O.J. Rojas, Fabrication and characterization of bactericidal thiol-chitosan and chitosan iodoacetamide nanofibres, Int. J. Biol. Macromol. 94 (2017) 96–105.
[25] T.J. Sill, H.A. von Recum, Electrospinning: applications in drug delivery and tissue engineering, Biomaterials. 29 (2008) 1989–2006.
[26] F. Dabirian, S.A.H. Ravandi, A.R. Pishevar, R.A. Abuzade, A comparative study of jet formation and nanofiber alignment in electrospinning and electrocentrifugal spinning systems, J. Electrost. 69 (2011) 540–546.
[27] J.M. Deitzel, J. Kleinmeyer, D.E.A. Harris, N.C.B. Tan, The effect of processing variables on the morphology of electrospun nanofibers and textiles, Polymer (Guildf.) 42 (2001) 261–272.
[28] J. Fang, X. Wang, T. Lin, Functional applications of electrospun nanofibers, Nanofibers Prod. Prop. Funct. Appl. 14 (2011) 287–302.
[29] S.A. Hosseini Ravandi, C. Gandhimathi, M. Valizadeh, S. Ramakrishna, Application of electrospun natural biopolymer nanofibers, Curr. Nanosci. 9 (2013) 423–433.
[30] S. Yadav, M.P. Illa, T. Rastogi, C.S. Sharma, High absorbency cellulose acetate electrospun nanofibers for feminine hygiene application, Appl. Mater. Today 4 (2016) 62–70.
[31] S. Sharaf, M.E. El-Naggar, Eco-friendly technology for preparation, characterization and promotion of honey bee propolis extract loaded cellulose acetate nanofibers in medical domains, Cellulose. 25 (2018) 5195–5204, https://doi.org/10.1007/s10570-018-1921-1.
[32] S. Tungprapa, I. Jangchud, P. Supaphol, Release characteristics of four model drugs from drug-loaded electrospun cellulose acetate fiber mats, Polymer (Guildf.) 48 (2007) 5030–5041.
[33] R. Konwarh, N. Karak, M. Misra, Electrospun cellulose acetate nanofibers: the present status and gamut of biotechnological applications, Biotechnol. Adv. 31 (2013) 421–437, https://doi.org/10.1016/j.biotechadv.2013.01.002.
[34] W. Zhou, J. He, S. Cui, W. Gao, Studies of electrospun cellulose acetate nanofibrous membranes, Open Mater. Sci. J. 5 (2011).
[35] D.S. Bajwa, G. Pourhashem, A.H. Ullah, S.G. Bajwa, A concise review of current lignin production, applications, products and their environmental impact, Ind. Crop. Prod. 139 (2019), 111526.
[36] V.J. Kim, C.K. Okano, C.R. Osborne, D.M. Frank, C.T. Meana, M.S. Castaneto, Can synthetic urine replace authentic urine to "beat" workplace drug testing? Drug Test. Anal. 11 (2019) 331–335.
[37] A.M. El Nahrawy, A.B.A. Hammad, A.M. Bakr, B.A. Hemdan, A.R. Wassel, Decontamination of ubiquitous harmful microbial lineages in water using an innovative Zn2Ti0.8Fe0.2O4 nanostructure: dielectric and terahertz properties, Heliyon. 5 (2019), https://doi.org/10.1016/j.heliyon.2019.e02501.
[38] A.M. El Nahrawy, B.A. Hemdan, A.B. Abou Hammad, A.M. Othman, A. M. Abouelnaga, A.M. Mansour, Modern template design and biological evaluation of cephradine-loaded magnesium calcium silicate nanocomposites as an inhibitor for nosocomial bacteria in biomedical applications, Silicon. (2020) 1–13.
[39] B.A. Hemdan, A.M. El Nahrawy, A.-F.M. Mansour, A.B.A. Hammad, Green sol–gel synthesis of novel nanoporous copper aluminosilicate for the eradication of pathogenic microbes in drinking water and wastewater treatment, Environ. Sci. Pollut. Res. 26 (2019), https://doi.org/10.1007/s11356-019-04431-8.
[40] M. He, T. Wu, S. Pan, X. Xu, Antimicrobial mechanism of flavonoids against Escherichia coli ATCC 25922 by model membrane study, Appl. Surf. Sci. (2014), https://doi.org/10.1016/j.apsusc.2014.03.125.
[41] B.A. Hemdan, M.A. El-Liethy, M.E.I. ElMahdy, G.E. El-Taweel, Metagenomics analysis of bacterial structure communities within natural biofilm, Heliyon. 5 (2019), e02271.
[42] K.T. Joshi, A.M. Pancholi, Synthesis, characterization and antibacterial activity of complexes of Schiff bases derived from 2-amino-5-methyl-4-phenyl thiazole and heterocyclic ketone/b-diketone, Orient. J. Chem. 16 (2000) 287–290.
[43] P.G. More, R.B. Bhalvankar, Synthetic, spectral, thermal and antibacterial studies on copper (II) and zinc (II) complexes using NNO donor Schiff bases, J. Indian Chem. Soc. 81 (2004) 13–17.
[44] C.L. Salas Araujo, Soy-based Polymers for Surface Modification and Interactions With Lignocellulosic Materials, 2013.
[45] T. Białopiotrowicz, B. Jańczuk, The wettability of a cellulose acetate membrane in the presence of bovine serum albumin, Appl. Surf. Sci. 201 (2002) 146–153.
[46] C. Liu, R. Bai, Preparation of chitosan/cellulose acetate blend hollow fibers for adsorptive performance, J. Membr. Sci. 267 (2005) 68–77.
[47] D. Kun, B. Pukánszky, Polymer/lignin blends: interactions, properties, applications, Eur. Polym. J. 93 (2017) 618–641.
[48] C. Wang, S.S. Kelley, R.A. Venditti, Lignin-based thermoplastic materials, ChemSusChem. 9 (2016) 770–783.
[49] N. Ghazy, S. El-Nahrawy, Siderophore production by Bacillus subtilis MF497446 and Pseudomonas koreensis MG209738 and their efficacy in controlling Cephalosporium maydis in maize plant, Arch. Microbiol. 203 (2021) 1195–1209.
[50] A. Temitayo Olufunmilayo, O. Isaac Ayoola, A. Adeleke Clement, O. Grace Olufunmilayo, O. Olayinka, A. Ezekiel Olugbenga, A. Adebowale Olusoji, Synthesis, characterization and antimicrobial activities of some metal (II) amino acids' complexes, Adv. Biol. Chem. 2012 (2012).
[51] M.R. Das, R.K. Sarma, S.C. Borah, R. Kumari, R. Saikia, A.B. Deshmukh, M. V. Shelke, P. Sengupta, S. Szunerits, R. Boukherroub, The synthesis of citrate-modified silver nanoparticles in an aqueous suspension of graphene oxide nanosheets and their antibacterial activity, Colloids Surf. B: Biointerfaces 105 (2013) 128–136.
[52] G. Jiang, X. Li, Y. Che, Y. Lv, F. Liu, Y. Wang, C. Zhao, X. Wang, Antibacterial and anticorrosive properties of CuZnO@RGO waterborne polyurethane coating in circulating cooling water, Environ. Sci. Pollut. Res. (2019), https://doi.org/10.1007/s11356-019-04374-0.
[53] A.M. El Nahrawy, B.A. Hemdan, A.B. Abou Hammad, Morphological, impedance and terahertz properties of zinc titanate/Fe3+ nanocrystalline for suppression of Pseudomonas aeruginosa biofilm, Nano Struct. Nano Objects 26 (2021), 100715.
[54] H.R.M. Rashdan, A.H. Abdelmonsef, M.M. Abou-Krisha, T.A. Yousef, Synthesis, identification, computer-aided docking studies, and ADMET prediction of novel benzimidazo-1, 2, 3-triazole based molecules as potential antimicrobial agents, Molecules. 26 (2021) 7119.
[55] W.A. Khalil, H.H.A. Sherif, B.A. Hemdan, S.K.H. Khalil, W. El Hotaby, Biocompatibility enhancement of graphene oxide-silver nanocomposite by functionalisation with polyvinylpyrrolidone, IET Nanobiotechnol. 13 (2019) 816–823.